X-Sieve: CMU Sieve 2.2
Resent-Date: Wed, 28 Sep 2005 08:54:34 -0500
Resent-To: Jeremy Bennett <jebennet@indiana.edu>
From: Larry Brewer <brewer1@llnl.gov>
Subject: Faculty Application
Resent-From: Yves Brun <ybrun@indiana.edu>
Date: Mon, 26 Sep 2005 15:56:16 -0700
To: ybrun@indiana.edu
X-Mailer: Apple Mail (2.623)

Dear Dr. Brun, I am applying for a faculty position in the Department of Biology at Indiana University. My area of research specialty is understanding the higher order structure of the sperm genome and how it is packaged using "single molecule", biophysical techniques. I have included my CV and Research Interests, as well as five of my most recent papers, all in pdf format. I am especially interested in multidisciplinary research and I have a strong background in both physics and biology. I have just performed the first measurements of the forces exerted by sperm nuclear proteins as they bind to DNA and they are large, some tens of pN, which is amazing in that no ATP is utilized. I think that my research would fit in well at the Biocomplexity Institute. Thanks for your consideration. Sincerely,

Dr. Laurence R. Brewer
Lawrence Livermore National Laboratory
Livermore, CA 94550
Tel: (925) 423-2343
Mobile: (510) 847-0363

 CURRICULUM VITAE 11.pdf

 Research Interests.pdf

 SCIENCE99.PDF

 NATURE.PDF

 JBC02.pdf

 JBC03.pdf

 BIOPHYJ03.pdf

Laurence R. Brewer

Research Interests

A Force-Exerting Nanomachine Coils DNA in Sperm.

The concentration of genomic DNA in the sperm cell is higher than that of any other cell. Unlike the chromatin in somatic cells, which is packaged in the form of nucleosomes, the DNA in the sperm cell of vertebrates is packaged by the protein protamine into 50-nm diameter toroids. However, no light has been shed on the mechanisms of toroid formation or genome compaction until recently, when we used single molecule techniques to measure the compaction forces produced during the formation of individual toroids.

We have measured dramatic increases in tension (Fig. 2) produced by the binding of protamine to a constrained lambda-phage DNA molecule (Fig. 1). The increase in tension is due to the neutralization of the DNA negative backbone by the highly charged protamine (21^{+}). Once protamine binds to DNA and forms a toroid it then locks it into place as shown in Fig. 3. *These forces almost certainly play a role in compaction of the sperm genome during spermiogenesis,* when the volume of the cell is decreased by over 60-fold. These changes are striking in that protamine does not use ATP as an energy source but instead relies on neutralizing DNA causing it to become highly hydrophobic. We have also shown that protamine only binds to DNA that is bent (data not shown) and forms a toroid out of slack DNA, increasing the DNA tension until no more protamine can bind. . A thermal "ratchet and pawl" mechanism likely reels in the DNA, much like a garden hose.

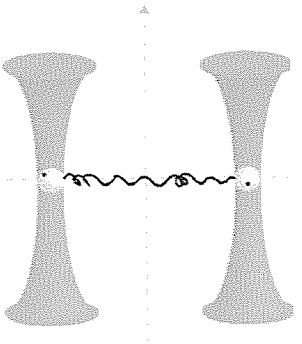

Fig. 1 Dual optical traps hold a lambda-phage DNA molecule via attached 0.93 μm beads. The DNA tension is measured via the displacement of one of the trapped beads.

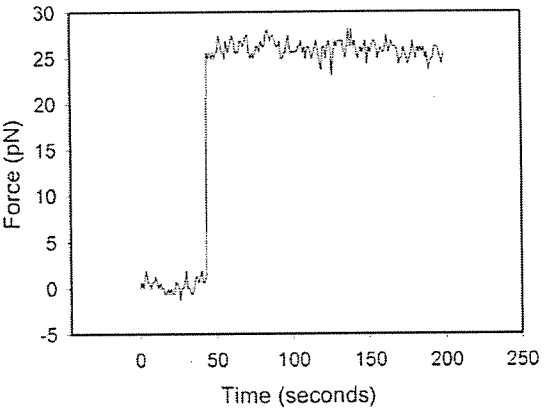

Fig. 2 Change in tension of a lambda-phage DNA molecule (16.5 μm contour length) held at 6 μm extension initially in buffer (0-50 seconds) and then in 5 μM salmine protamine.

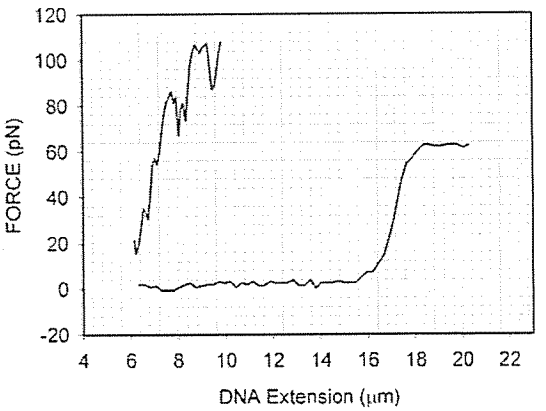

Fig. 3 Elasticity of a single lambda-phage DNA molecule in buffer showing the characteristic overstretching transition at 60 pN (black) and in 5 μM salmine protamine (blue).

Mimicking Cellular Processes in Microfluidic Flow-Cells

Multichannel flow-cells allow one to measure changes in both the shape and tension of a single DNA molecule as it is exposed to proteins, enzymes or reagents. The flow cell allows the concentrations of protein to be kept constant and the flow speed to be controlled precisely. An example of an experiment utilizing a two -channel flow cell is shown in Fig. 4. below. A single DNA molecule is moved from one side of the flow cell to another using an optical trap. An intercalating dye allows one to observe real-time structural changes in DNA molecule as protein binds to it and thus measure on-rates, off-rates and equilibrium constants (*1, 2*).

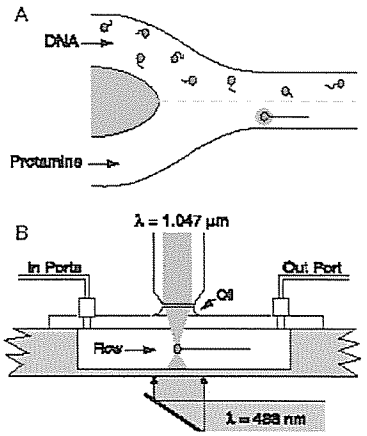

Fig. 4 A) Single DNA molecules attached to 1 μm beads flow into one channel of a two-channel flow cell and protamine flows in through the second channel with little mixing. **B)** The DNA molecule is held by an optical trap and stained with the intercalating dye YOYO-1 allowing it to be imaged using fluorescence micrscopy.

Two and three channel flow cells that we have manufactured are shown in Figs. 5 and 6. These flow cells can also be used to measure changes in DNA structure due to the binding of proteins using two optical traps, as described in the previous section.

We are interested in using flow cells to exactly mimic *in vivo* cellular processes. We will use a multichannel flow cell with a large number of channels (>5) so that a single DNA molecule can interact with a large number of proteins in the same sequence that occurs during a particular process in the cell.

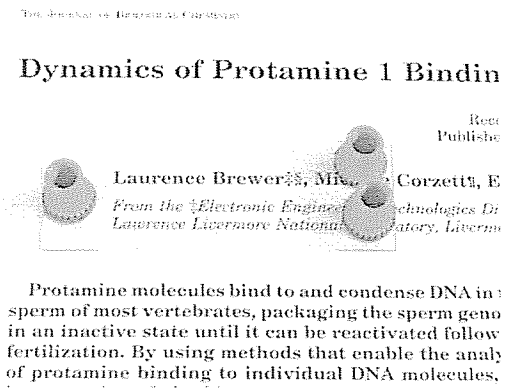
Dynamics of Protamine 1 Bindin

Laurence Brewer[illegible], Mic[illegible] Corzett, E

Protamine molecules bind to and condense DNA in sperm of most vertebrates, packaging the sperm geno in an inactive state until it can be reactivated follow fertilization. By using methods that enable the analy of protamine binding to individual DNA molecules,

Fig. 5 Two-channel flow cell formed using anodic bonding.

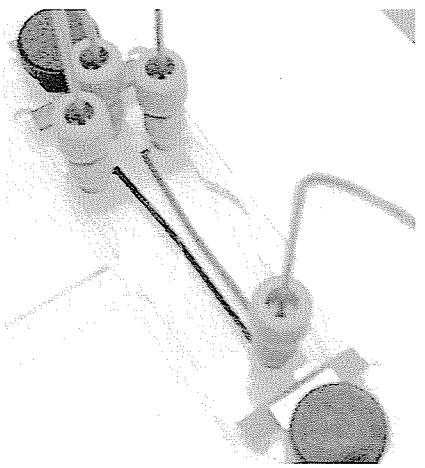

Fig. 6 Three-channel flow cell formed using PDMS replica molding. Red, white and blue dyes flow laminarly, side by side with little mixing.

Measurement of the Helical State of a Single DNA Molecule

The helical state of DNA plays an important role in many fundumental biological processes including replication, transcription, recombination, and repair. We are currently building an instrument to measure changes in the twist of a single DNA molecule suspended between two optical traps as shown in Fig. 1. The optical traps form frictionless swivels for the beads attached at each end of the DNA molecule. Each of the beads will be decorated with a 40-nm fluorescent microsphere or quantum dot. If there are any changes in the helical state of DNA, due to for instance, DNA unwinding or supercoiling, these topological changes must be transmitted to the ends of the DNA molecule and the attached beads will rotate in opposite directions. This process can be envisioned by pulling on the ends of a phone cord. As the coils start to become unwound you will be able to feel the ends of the phone cord rotate in opposite directions. Fig. 7 shows a tiled series of images taken in our lab of a 0.93 μm bead decorated with a 40 nm fluorescent microsphere, rotating randomly in an optical trap due to Brownian motion. We hope to use this instrument to study how histones are displaced from nucleosomal DNA during spermiogenesis, and how the binding of proteins to promoter sites affects the helical state of DNA during transcription.

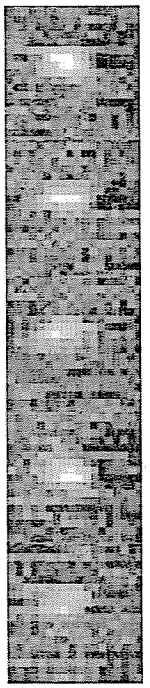

Fig. 7 Random rotations of a 0.93 μm bead due to Brownian motion are observed via an attached 40-nm fluorescent nanosphere. This will be used to measure changes in the twist and writhe of a single DNA molecule.

References

1. L. R. Brewer, M. Corzett, R. Balhorn, *Science* **286**, 120-3 (Oct 1, 1999).
2. P. R. Bianco *et al.*, *Nature* **409**, 374-8 (Jan 18, 2001).

additional intervening protein or proteins. These experiments may have also uncovered an additional role for Est1 in telomerase function, as the Cdc13-Est2 fusion was not capable of promoting extensive telomere elongation in the absence of Est1 (Fig. 3C) (*26*). Because Est1 is a terminus-specific DNA binding protein (*11*), we speculate that this second role may be to promote accessibility of the 3′ terminus to the active site of telomerase.

References and Notes

1. C. I. Nugent and V. Lundblad, *Genes Dev.* **12**, 1073 (1998).
2. J. Shampay and E. H. Blackburn, *Proc. Natl. Acad. Sci. U.S.A.* **85**, 534 (1988).
3. S. Marcand, E. Gilson, D. Shore, *Science* **275**, 986 (1997); B. van Steensel and T. de Lange, *Nature* **385**, 740 (1997); S. Marcand, V. Brevet, E. Gilson, *EMBO J.* **18**, 3509 (1999).
4. C. I. Nugent, T. R. Hughes, N. F. Lue, V. Lundblad, *Science* **274**, 249 (1996).
5. V. Lundblad and J. W. Szostak, *Cell* **57**, 633 (1989).
6. T. S. Lendvay, D. K. Morris, J. Sah, B. Balasubramanian, V. Lundblad, *Genetics* **144**, 1399 (1996).
7. M. S. Singer and D. E. Gottschling, *Science* **266**, 404 (1994).
8. J. Lingner *et al.*, *ibid.* **276**, 561 (1997).
9. M. Cohn and E. H. Blackburn, *ibid.* **269**, 396 (1995).
10. J. Lingner, T. R. Cech, T. R. Hughes, V. Lundblad, *Proc. Natl. Acad. Sci. U.S.A.* **94**, 11190 (1997).
11. V. Virta-Pearlman, D. K. Morris, V. Lundblad, *Genes Dev.* **10**, 3094 (1996).
12. J. J. Lin and V. A. Zakian, *Proc. Natl. Acad. Sci. U.S.A.* **93**, 13760 (1996).
13. B. Garvik, M. Carson, L. Hartwell, *Mol. Cell. Biol.* **15**, 6128 (1995).
14. T. R. Hughes, S. K. Evans, R. G. Weilbaecher, V. Lundblad, in preparation.
15. In-frame fusion proteins were constructed as follows: The Cdc13-Est1 fusion (pVL1091) fused $Cdc13_{1-924}$-$Est1_{6-699}$; the Cdc13-Est2 (pVL1107) and Cdc13-$Est2_{D670A}$ (pVL1111) proteins fused $Cdc13_{1-924}$-$Est2_{1-884}$. All three constructs were expressed from the genomic *CDC13* promoter and derived from the single-copy *CEN* plasmid, pRS415. The Est1-DBD_{Cdc13} and Est1-47-DBD_{Cdc13} fusions (pVL1120 and pVL1121, respectively), expressed in single copy from the *EST1* promoter, fused the Cdc13 DNA binding domain (*22*) to the COOH terminus of Est1, to generate $Est1_{1-699}$ - $Cdc13_{2-21,452-693}$. Telomere elongation by any of these fusion proteins is not due to increased protein expression in the context of the fusion, because overexpression of Est1, Est2, or Cdc13, or expression of Est1 by the *CDC13* promoter, has little or no effect on telomere length (*8*, *11*, *17*, *19*).
16. We have also observed up to a ~4-kb increase in the length of a single telomere (chromosome IIIL). Strains with greatly elongated telomeres do not exhibit any discernable growth defect but were not examined for more subtle defects (such as alterations in cell cycle progression). We have not investigated yet whether the increase in telomere length in strains carrying Cdc13-telomerase fusions occurs at a constant rate, or if there is some influence of cis-inhibition on elongation, as previously observed (*3*).
17. S. K. Evans and V. Lundblad, unpublished data.
18. The *est1-47* mutation is one of a panel of alanine-scan mutations in *EST1* (*17*); the Est1-47 mutant protein still retains association with telomerase (at 20% of WT levels), as assessed by coimmunoprecipitation with the TLC1 RNA (*27*).
19. N. Grandin, S. I. Reed, M. Charbonneau, *Genes Dev.* **11**, 512 (1997).
20. A. Chandra, T. R. Hughes, V. Lundblad, unpublished data.
21. C. I. Nugent, E. Pennock, V. Lundblad, unpublished data.
22. T. R. Hughes, R. G. Weilbaecher, V. Lundblad, in preparation.
23. Previous work showed that high-level expression of the $Est2_{D670A}$ mutant protein (under the control of the *ADH* promoter, on a 2μ high-copy plasmid) resulted in substantially shorter telomeres in an *EST2*$^+$ strain (*8*). The lack of an effect of the Cdc13-$Est2_{D670A}$ fusion on WT telomere length (Fig. 3A) is presumably a consequence of the lower levels of this fusion protein (confirmed by protein immunoblotting analysis), due to single-copy plasmid expression by the *CDC13* promoter. As expected, the Cdc13-$Est2_{D670A}$ fusion failed to complement an *est2-Δ* strain.
24. Bypass of *est1-Δ* senescence was not simply a consequence of increased Est2 levels (due to possible minimal increase in expression of *EST2* by the *CDC13* promoter), because even higher level expression of *EST2* by the constitutive *ADH* promoter (*8*) was not sufficient to allow an *est1-Δ* strain to grow (*17*).
25. V. Lundblad and E. H. Blackburn, *Cell* **73**, 347 (1993).
26. Association of Cdc13-Est2 fusion protein with the TLC1 RNA was reduced by less than twofold in the absence of Est1, as assessed by immunoprecipitation (*27*), arguing that the failure to elongate telomeres in an *est1-Δ* strain is not simply due to reduced stability of the Cdc13-Est2 telomerase complex.
27. For each sample, cells were grown in selective media to an optical density (600 nm) of 1.0. Cells were harvested by centrifugation and the cell pellets were washed in water and then in TMG 300÷ [10 mM tris-HCl (pH 8.0), 1 mM $MgCl_2$, 5% glycerol, 1 mM phenylmethylsulfonyl fluoride, 300 mM NaCl]. Cell extracts were prepared by five repeated cycles of freezing and grinding in liquid nitrogen. Extracts were cleared twice by centrifugation for 10 min at 14,000 rpm at 4°C and immunoprecipitated with an antibody to hemagglutinin (HA) (16β12, Babco) and protein A/G agarose beads (Calbiochem). RNA was prepared by SDS–phenol-chloroform extraction, and TLC1 was detected on 7 M urea–4% polyacrylamide gel as described (*8*). The efficiency of TLC1 recovery in immunoprecipitates is typically less than 2%; the recovery with untagged proteins was less than 0.05%.

28. We thank T. Hughes, R. Weilbaecher, and L. Zumstein for critical review of the manuscript. Supported by NIH grant RO1GM55867 (V.L.) and by a U.S. Army Breast Cancer Research Predoctoral Traineeship (S.K.E.).

9 June 1999; accepted 30 August 1999

Protamine-Induced Condensation and Decondensation of the Same DNA Molecule

Laurence R. Brewer,[1] Michele Corzett,[2] Rod Balhorn[2]

The DNA in sperm and certain viruses is condensed by arginine-rich proteins into toroidal subunits, a form of packaging that inactivates their entire genome. Individual DNA molecules were manipulated with an optical trap to examine the kinetics of torus formation induced by the binding of protamine and a subset of its DNA binding domain, Arg_6. Condensation and decondensation experiments with λ-phage DNA show that toroid formation and stability are influenced by the number of arginine-rich anchoring domains in protamine. The results explain why protamines contain so much arginine and suggest that these proteins must be actively removed from sperm chromatin after fertilization.

Protamine and other polycations have been shown to coil DNA into toroidal structures containing up to 60 kb of DNA (*1–3*). Individual bacteriophage appear to contain a single toroid folded inside the protein capsid (*3*), whereas a sperm cell contains as many as 50,000 toroids packed inside its nucleus (*1*). The protamines responsible for inducing torus formation and packaging DNA in maturing spermatids contain a series of arginine-rich anchoring domains (*4*) that bind to the phosphodiester backbone of DNA in a base sequence–independent fashion (*5*). One protamine molecule is bound to each turn [~11 base pairs (bp)] of DNA (*5*, *6*), and adjacent arginines in the anchoring domains interlock both strands of the helix. Arginine-rich sequences are also present in the proteins that package DNA in several viruses (*7*), but the viral proteins contain fewer anchoring domains per molecule.

In vitro studies using light scattering (*8*, *9*), electron and atomic force microscopy (*1*, *2*, *10*), fluorescence microscopy (*11*, *12*), and DNA elasticity measurements (*13*) have examined how protamine and other polycations induce torus formation. The interpretation of light-scattering experiments has been complicated by DNA aggregation, whereas electron and atomic force microscopy studies characterized only the structure of the final product. Toroid formation and the kinetics of the condensation process could not be observed by fluorescence microscopy because the molecules were not sufficiently extended. To examine toroid formation under conditions that preclude aggregation and precipitation and allow a detailed analysis of kinetics, we used an optical trap to isolate individual DNA molecules and fluorescence microscopy to monitor the formation of toroids in real time

[1]Electronics Engineering Technologies Division, [2]Biology and Biotechnology Research Program, Lawrence Livermore National Laboratory, Livermore, CA 94550, USA.

as they are induced by protamine (or Arg_6) binding.

λ-phage DNA concatemers (20 to 80 μm long) were tagged at one end with a biotinylated oligonucleotide attached to a 1-μm streptavidin-coated polystyrene bead and stained with the intercalating dye YOYO-1 (*14*). These molecules were introduced through one port of a "bifurcated flow cell" (Fig. 1A) and the condensing agent protamine (or Arg_6) through another port so that the two solutions flowed side by side with minimal mixing. An infrared optical trap (*15*) (Fig. 1B) was used to move an individual DNA molecule, via its attached bead, from the sample (DNA) side to the condensing agent (protein) side of the flow cell. The molecule was extended by the force of the flowing buffer, and its entire length became visible because of the fluorescence of the intercalated dye. Toroid formation (condensation) (Fig. 1C) was monitored in real time by measuring the change in length of the molecule as a function of time after moving it into the buffer stream containing protein (*16*).

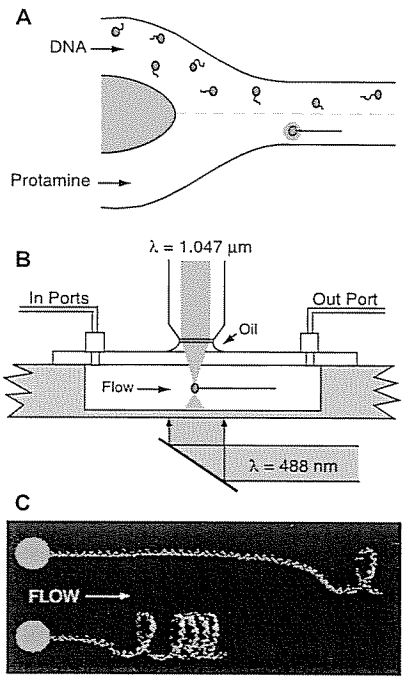

Fig. 1. (**A**) Top view of the flow cell (*25*) showing how the DNA molecules (attached to beads) and protamine enter the cell and form an interface (– – –) with little or no mixing. (**B**) Side view of the system showing the optical trap (orange) holding a bead attached to a single DNA molecule. The cell is illuminated from beneath by a 1-mW argon-ion laser, λ = 488 nm, to excite the YOYO-1 dye bound to the DNA. (**C**) Model of a DNA molecule condensing in protamine (protamine molecules not shown). The upper molecule shows the initiation of coiling and the lower molecule depicts the progression of coiling to form the torus.

Images documenting the progression of condensation for a 50-μm DNA concatemer in protamine (*17*) are shown in Fig. 2. The toroid, which appeared as a bright spot at the end of the DNA molecule, increased in brightness as it moved toward the bead. In 1.1 μM protamine, the condensation process was completed in ~19 s. The change in length versus time for four different DNA molecules as they condensed in different concentrations of protamine is shown in Fig. 3A. As long as the DNA was extended by flow, torus formation initiated at the free end of the molecule, and its length decreased linearly with time, as predicted by Ostrovsky and Bar-Yam (*18*). The movement of the toroid often exhibited a jerky, start-and-stop motion, but when the process was repeated with the same DNA molecule (Fig. 4) this motion was not reproduced. Although these sporadic fluctuations in condensation rate cannot be DNA sequence or conformation dependent, they may relate to the cooperative nature of protamine binding and a nonrandom, incomplete coverage of the DNA molecule that develops as the protamines bind. Condensation (toroid movement) should decrease or stop if the toroid encountered regions that were not completely covered by protamine.

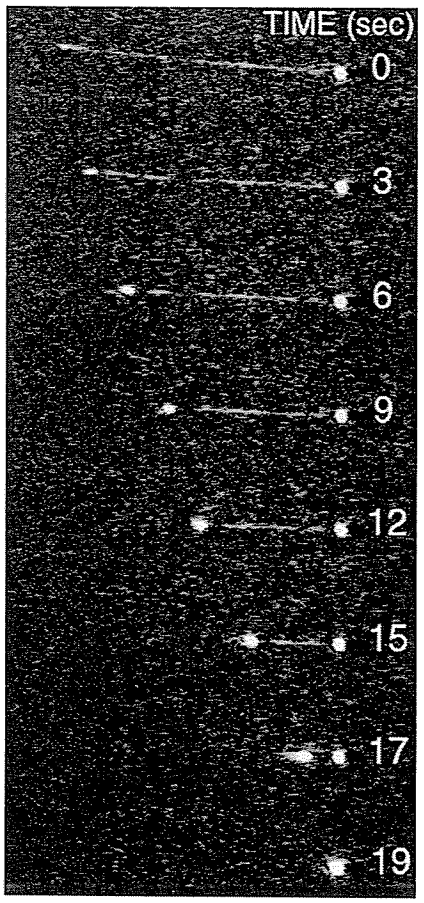

Fig. 2. Progression of condensation of a 50-μm concatemer of λ-phage DNA attached to a 1-μm bead. The bead was held stationary by an optical trap and the DNA molecule is extended by the flow of the incoming buffer containing 1.1 μM protamine (v = 17.6 μm/s). Each time frame was captured after initiation of condensation as shown.

Experiments conducted at different protamine concentrations showed that the rate of condensation was limited by the rate of protamine binding to the DNA molecule. The change in rate (Fig. 3B) was linear, with a slope of 2.6 ± 0.47 μm/μM-s. This corresponds to a rate of protamine binding to DNA of 600 ± 110 molecules/μM-s. The rate of condensation was measured at two different concentrations of YOYO-1 (0.1 and 0.02 μM) to determine whether intercalated YOYO-1 molecules affect the condensation rate. No statistically significant difference in the rates was observed. The potential effect of buffer flow and its frictional force on toroid movement was also assessed by calculating the force that would be exerted on a sphere of equivalent volume to the toroid and by performing an experiment to test the effect of the force directly. The force was calculated by Stokes' law to be 0.43 pN (*19*). The effect of the force was determined experimentally by comparing the condensation rates measured for 30 DNA molecules condensed in 1.5 μM protamine over a range of buffer flow rates (20 to 70 μm/s). The slope of the fitted line through the data points (0.00 ± 0.038) indi-

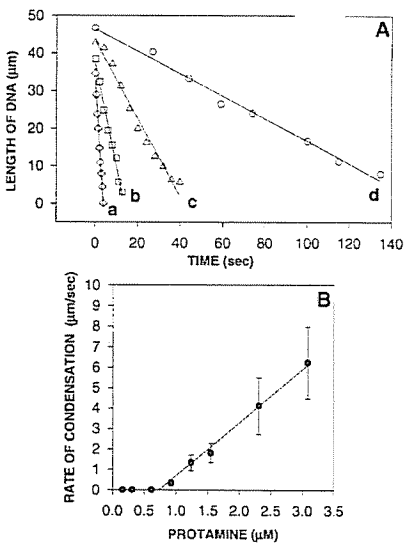

Fig. 3. (**A**) Change in length versus time measured for four different DNA molecules condensed in a different protamine concentration (flow speed, v = 50 μm/s): (**a**) 3.1 μM (diamonds); (**b**) 1.6 μM (squares); (**c**) 1.2 μM (triangles); (**d**) 0.93 μM (circles). Lines are least-squares fits to the data points. (**B**) Condensation rates were determined by collecting data for about 200 individual DNA molecules condensed by protamine.

cated that the condensation rate was not affected by the velocity of the buffer flow.

To estimate the off-rate of protamine, we measured the decondensation rates of individual condensed DNA molecules after moving them back to the DNA side of the flow cell. We monitored decondensation, which occurs only when protamine dissociates from the DNA, for periods up to 25 min and used the lengthening (uncoiling) of the molecule to estimate the rate of protamine dissociation. The measured rate of increase in DNA length, 3.1 ± 1.3 nm/s, corresponds to a protamine off-rate of 0.71 molecule per second (*20*). At this rate, the complete dissociation of protamine from the sperm genome (1.5×10^9 bp) would require at least 6 years. Because sperm chromatin takes only 5 to 10 min to decondense after fertilization, these results support the hypothesis that protamine must be actively removed from DNA (*21*) once the chromatin enters the egg's cytoplasm. The protamine dissociation constant derived from these measurements, 1.17 ± 0.53 nM, is similar to values obtained by others for herring protamine (1.25 nM and 1.15 nM) with bulk DNA (*9, 22*).

Similar studies conducted with Ac-RRRRRR-amide (Arg_6), one of three Arg_6 anchoring domains present in protamine, revealed that a 68-fold higher concentration of Arg_6 (160 μM) was required to achieve a condensation rate comparable to that measured for protamine (4.2 ± 1.1 μm/s). This suggests that either Arg_6 has a much lower binding affinity for DNA, or the consecutive binding of three individual Arg_6 molecules is statistically much less likely than the binding of a single protamine molecule. In contrast to the protamine complexes, DNA molecules condensed by Arg_6 decondensed rapidly when pulled back across the interface and out of the buffer containing the peptide. Four successive condensation-decondensation measurements performed on the same molecule in 107 μM Arg_6 are shown in Fig. 4. The mean condensation rate for these four measurements was 9.1 ± 2.5 μm/s, and the mean decondensation rate was 21.25 ± 2.9 μm/s. Because the Arg_6 molecule binds to only 3 bp of DNA, these data indicate that the off-rate for Arg_6 is 18×10^3 molecules per second—four orders of magnitude higher than the off-rate of protamine (*23*). The dissociation constant, 0.25 ± 0.08 mM, has not been measured previously.

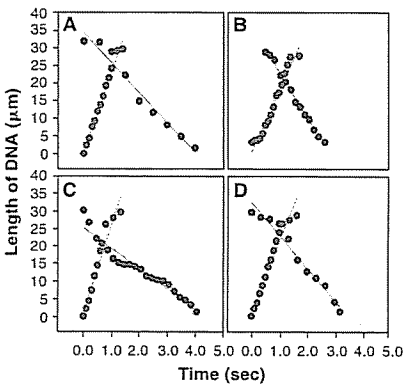

Fig. 4. Condensation (blue dots) and decondensation (red dots) of the same DNA molecule in 107 μM Arg_6 (flow speed, v = 28 μm/s) performed four successive times (**A** to **D**).

Experiments conducted with concatemers of different lengths also indicated that there may be a limit to the amount of DNA that can be coiled into a toroid. Only one toroid was observed during the condensation of single λ-phage DNA molecules, whereas multiple toroids (Fig. 5) were observed when concatemers containing two to four molecules were condensed at a low flow rate (v < 10 μm/s). Although additional experiments must be conducted to verify the maximum length of sequence that can be coiled into a torus, the present studies suggest that one torus is formed for each length of λ-phage DNA (48.5 kb). Although it is not clear why such a limit should exist, this estimate (~50 kb) is close to the 60 kb derived from toroid volumes measured by electron microscopy (*10*).

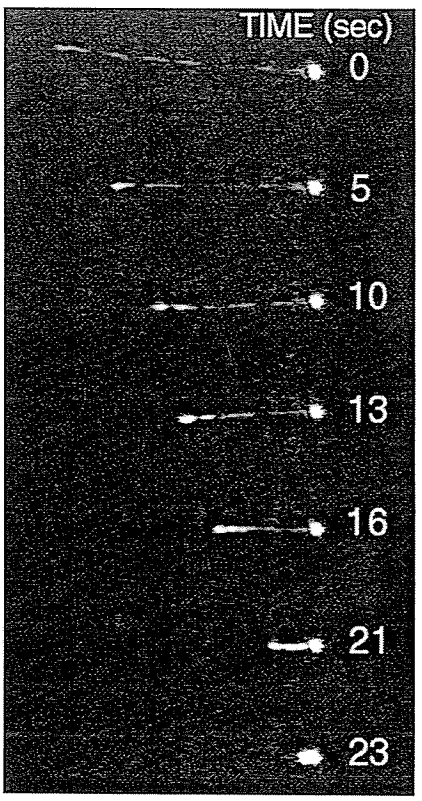

Fig. 5. Condensation of a 45-μm concatemer of λ-phage DNA attached to a 1-μm bead held stationary by an optical trap in 1.1 μM protamine (flow speed, v = 6.1 μm/s). Three toroids were observed to form, sequentially starting at the free end of the DNA molecule.

By combining the use of an optical trap, a dual-port flow cell, and single molecule imaging, we have examined the condensation kinetics of individual DNA molecules, obtained estimates of the binding and dissociation rates for protamine and Arg_6 in the absence of competing aggregation reactions, and monitored the formation and motions of toroids in real time to obtain results that only single molecule studies can provide. In addition to providing new insight into the mechanism of DNA condensation by protamine, this work presents an example of how experiments with single DNA molecules can be used to study the kinetics and biophysics of protein-DNA interactions.

References and Notes

1. N. V. Hud, M. J. Allen, K. H. Downing, J. Lee, R. Balhorn, *Biochem. Biophys. Res. Commun.* **193**, 1347 (1993).
2. R. Balhorn *et al.*, in *The Male Gamete: From Basic Science to Clinical Applications*, C. Gagnon, Ed. (Cache River Press, Vienna, IL, 1999), pp. 55–70.
3. K. E. Richards, R. C. Williams, R. Calender, *J. Mol. Biol.* **78**, 255 (1973); S. M. Klimenko, T. I. Tikchonenko, V. M Andreev, *ibid.* **23**, 523 (1967); N. V. Hud, *Biophys. J.* 69, 1355 (1995).
4. R. Balhorn, in *Molecular Biology of Chromosome Function*, K. W. Adolph, Ed. (Springer-Verlag, New York, 1989), p. 366.
5. N. V. Hud, F. P. Milanovich, R. Balhorn, *Biochemistry* **33**, 7528 (1994).
6. G. S. Bench, A. M. Friz, M. H. Corzett, D. H. Morse, R. Balhorn, *Cytometry* **23**, 263 (1996).
7. T. M. Cao, M. T. Sung, *Biochem. Biophys. Res. Commun.* **108**, (1982); S. Maeda, S. G. Kamita, H. Kataoka, *Repeat. Virol.* **180**, 807 (1991).
8. J. Widom and R. L. Baldwin, *J. Mol. Biol.* **144**, 431(1980); C. B. Post and B. H. Zimm, *Biopolymers* **21**, 2139 (1982); D. Porschke, *J. Mol. Biol.* **222**, 423 (1991).
9. F. Watanabe and G. Schwartz, *J. Mol. Biol.* **163**, 485 (1983).
10. P. G. Arscott, A. Li, V. A. Bloomfield, *Biopolymers* **30**, 619 (1990); V. A. Bloomfield, *ibid.* **44**, 269 (1998).
11. C. Bustamante, *Annu. Rev. Biophys. Biophys. Chem.* **20**, 415 (1991).
12. M. Ueda and K. Yoshikowa, *Phys. Rev. Lett.* **77**, 2133 (1996).
13. C. G. Baumann, S. B. Smith, V. A. Bloomfield, C. Bustamante, *Proc. Natl. Acad. Sci. U.S.A.* **94**, 6185 (1997).
14. λ-phage DNA molecules were labeled by annealing and ligating a 5′-biotin-labeled 12-base oligonucleotide (Genosys Biotechnologies Inc.) to the cos site. Concatemers of various lengths were formed by annealing unlabeled λ-phage DNA to the biotin-labeled DNA. The biotinylated DNA (2.2 μg) was attached to 1.8×10^8, 1-μm streptavidin beads (Interfacial Dynamics) in 100 mM $NaHCO_3$ (pH 8) at 37°C for 1 hour. The DNA-bead preparation was diluted to 0.2 μg/ml with degassed 50% (w/v) sucrose, 100 mM $NaHCO_3$ (pH 8), 30 mM dithiothreitol (DTT), 0.1 μM YOYO-1 (one dye molecule per 4 to 5 bp of DNA) and incubated for 2 hours before use. Salmon protamine (Sigma) was purified by high-pressure liquid chromatography and lyophilized. Arg_6 (SynPeP) was used as provided. The proteins were dissolved in 50% sucrose containing 100 mM $NaHCO_3$ (pH 8), diluted each day to the required concentrations in degassed 50% sucrose, 100 mM $NaHCO_3$ (pH 8), 30 mM DTT, and stored under nitrogen.
15. The optical trap was formed by focusing laser light from a solid-state Nd-YLF laser (λ= 1.047 μm, Spectra-Physics) through a Zeiss ×100 Plan Neofluor, oil immersion, infinite conjugate, objective. A Zeiss Ax-

ioplan microscope was modified by removing the illumination optics to allow entry of the laser. The typical laser power used to form the trap (exiting the microscope objective) was 50 mW.
16. The fluorescence was detected with an image-intensified charge-coupled device camera (PAULTEK), the signal was recorded on an SVHS VCR, and an Argus Image Processor (Hamamatsu) and a frame grabber (National Instruments PCI 1402) were used to perform background subtraction. The lengths of the DNA molecules, measured between the center of the 1-μm bead and the free end of the molecule, were obtained from frame-grabbed images. The length of stained DNA (48.5 kb) extended by flow was measured to be 19.2 ± 0.82 μm at a flow rate of 72 μm/s in 50% sucrose. Under these conditions, DNA is 93% extended (*24*).
17. The salmon protamine used in these experiments contains 21 positively charged arginines distributed throughout the length of the protein (32 amino acids).
18. B. Ostrovsky and Y. Bar-Yam, *Biophys. J.* **68**,1694 (1995).
19. Stokes' law, $f = 6\pi\eta rv$, where η is the buffer viscosity (15.4 cp), r is the sphere radius, and v is the buffer velocity (50 μm/s), was used to calculate the frictional force on the fully formed toroid. The toroid used to calculate the frictional force had a 90-nm outer diameter and a 30-nm inner diameter and was 20 nm thick (*1*).
20. Because we cannot confirm that every protamine has dissociated from the decondensed DNA molecule, these experiments provide only a maximum value for the off-rate.
21. S. A. Ruiz-Lara, L. Cornudella, A. Rodriguez-Campos, *Eur. J. Biochem.* **240**, 186 (1996).
22. M. Nakano *et al.*, *J. Biochem.* **105**, 133 (1989).
23. With an off-rate this high, molecules containing a single Arg_6 domain would remain bound to the sperm genome for only 2 hours. This is too short a period of time, because the protamine must remain bound to DNA and maintain the sperm chromatin in an inactive state for up to 2 weeks before fertilization.
24. T. T. Perkins, D. E. Smith, R. G. Larson, S. Chu, *Science* **268**, 83 (1995).
25. The flow cell contains two channels, each pumped at the same speed with a single syringe pump. The depth of the flow cell was 40 μm and the molecule was typically held 20 μm beneath the coverslip. Flow velocities were maintained at ~50 μm/s. Using a computer-controlled stage with 0.1-μm resolution to manipulate the position of the flow cell relative to the optical trap, we moved the DNA molecule to the protein side of the flow cell to initiate condensation.
26. Work was performed at Lawrence Livermore National Laboratory (LLNL) under the auspices of the U.S. Department of Energy under contract W-7405-ENG-48. Funding was provided by a LLNL Labwide Laboratory Directed Research Development Award. We thank J. Holzrichter, M. Colvin, and M. Cosman for their suggestions, support, and encouragement; J. W. Cosman and C. Barry for help during the early stages of the study; and J. T. Cosman for generating the computer graphics image of DNA.

1 April 1999; accepted 30 August 1999

Imidazole Rescue of a Cytosine Mutation in a Self-Cleaving Ribozyme

Anne T. Perrotta, I-hung Shih, Michael D. Been*

Ribozymes use a number of the same catalytic strategies as protein enzymes. However, general base catalysis by a ribozyme has not been demonstrated. In the hepatitis delta virus antigenomic ribozyme, imidazole buffer rescued activity of a mutant with a cytosine-76 (C76) to uracil substitution. In addition, a C76 to adenine substitution reduced the apparent pK_a (where K_a is the acid constant) of the self-cleavage reaction by an amount consistent with differences in the pK_a values of these two side chains. These results suggest that, in the wild-type ribozyme, C76 acts as a general base. This finding has implications for potential catalytic functions of conserved cytosines and adenines in other ribozymes and in ribonuclear proteins with enzymatic activity.

Transphosphoesterification reactions catalyzed by self-cleaving and self-splicing RNAs (ribozymes) require loss of a proton from the participating 2′- or 3′-hydroxyl group to promote its nucleophilic attack on the cleavage-site or splice-site phosphate (*1*, *2*). Metal ions can assist in this reaction, and metal-ion catalysis is one of several strategies that ribozymes share with protein enzymes (*1*, *2*). Enhanced nucleophilicity of the hydroxyl group could also result from base-catalyzed deprotonation (*1*–*3*). The pK_a values of the nucleoside side chains (pK_a ~ 3.5 to 4.5), however, appear to be too low to provide efficient general acid-base catalysis at physiologic pH (*4*). Although pK_a values can be shifted closer to neutrality in particular RNA structures (*2*, *5*), it has not been demonstrated that an RNA side chain can act as a general base in catalysis (*1*, *2*).

Department of Biochemistry, Box 3711, Duke University Medical Center, Durham, NC 27710 USA.

*To whom correspondence should be addressed. E-mail: been@biochem.duke.edu

The two hepatitis delta virus (HDV) ribozymes are structurally related self-cleaving RNAs (*6*, *7*) that require a 2′-hydroxyl group on the ribose located immediately 5′ of the cleavage site phosphate (*8*) and that generate products containing a 2′,3′-cyclic phosphate and a 5′-hydroxyl group (*9*). Thus, implied is a cleavage mechanism that involves nucleophilic attack of the 2′-hydroxyl or 2′-alkoxide on the cleavage-site phosphorus (Fig. 1). In the HDV ribozymes, a specific cytosine (C75 in the genomic ribozyme, designated γC75, and its counterpart C76 in the antigenomic ribozyme) has been hypothesized to accept the proton from the attacking 2′-hydroxyl group (*10*, *11*).

To establish that the cytosine base at position 76 was essential for cleavage in the antigenomic ribozyme, we tested whether exogenous cytosine could rescue activity of C76 mutants. We introduced mutations at C76 into the PEX1 antigenomic ribozyme sequence (*12*); consistent with previous findings (*13*), self-cleavage activity of C76u and C76g was undetectable under standard conditions (Fig. 2A). At 37°C, the rate constants were down by a factor of 10^6. Cleavage activity of the C76u ribozyme was partially restored when cytosine was added to the reaction mixture (*14*). Rescue of activity by exogenous bases and base analogs has previously been demonstrated in hammerhead ribozymes containing abasic residues (*15*). In those studies, rescue occurred through compensation of structural changes introduced by the abasic residue. To test whether cytosine rescue of the C76u mutant might reflect a catalytic role for the base, we substituted imidazole for cytosine. For C76u and C76g, addition of 200 mM imidazole (pH 7.4) to the reaction mixtures enhanced cleavage activity at least 250- and 25-fold, respectively (Fig. 2A and Table 1). The 3′ product band in these reactions was the same size as the normal 3′ product, which suggests that imidazole-dependent cleavage occurred at the wild-type cleavage site in the 101-nucleotide (nt) precursor. We tested several other buffers, but only imidazole and 4(5)-methylimidazole enhanced cleavage activity (*14*). A divalent cation (Mg^{2+}, Ca^{2+}, or Mn^{2+}) was required for cleavage of all constructs (Fig. 2A) (*16*).

Imidazole would most likely be acting as either a general base (pK_a ~ 7.0) or a nucleophile in the cleavage reaction. If imidazole acted as a nucleophile in a single-displacement reaction, it should show up in one of the products. However, a 2′,3′-cyclic phosphate would be generated if the adjacent 2′-hydroxyl was the nucleophile. Therefore, we characterized the 5′ cleavage product. For this analysis, the sequence 5′ to the cleavage site in both PEX1 and C76u was shortened from 8 to 3 nt. Wild-type and mutant precursor RNAs were 5′-end-labeled and allowed to cleave in the absence and presence of imidazole, respectively. The 5′ cleavage products for both ribozymes comigrated on polyacrylamide gels under denaturing conditions in which short fragments containing 3′(2′)-terminal phosphates were resolved from frag-

unless otherwise noted. TPM video-enhanced light microscopy, image recording, image processing and data analysis have been described[5–7]. TPM image acquisition time was 0.5 s.

χ-Recognition efficiency

The DNA substrates were made by treating *Nde*I-linearized pBR322 or pBR322 3χF, 3H with calf intestinal phosphatase, followed by 5′-end labelling using T4 polynucleotide kinase and [γ-^{32}P]ATP. Reactions were conducted at 25 °C essentially as described[20] and contained 25 mM Tris-acetate (pH 7.5), 1 mM $Mg(OAc)_2$, 1 mM DTT, 1 mM ATP, 1 mM ADP, 1.44 nM duplex DNA ends, 1.27 μM SSB and 0.4 nM active RecBCD-bio. The gels were dried then analysed on a phosphor imager; χ_3 recognition efficiency was taken to be the maximum value over measurements taken at different times of $2P_t/(R_0 - R_t)$ where R_t and P_t are the total radioactivity over background at time t in the unprocessed duplex substrate band and the long χ-specific product bands, respectively. This calculation underestimates the true recognition efficiency because an unknown fraction of the χ-specific products are further degraded during the reaction.

Received 23 August; accepted 7 November 2000.

1. Kuzminov, A. Recombinational repair of DNA damage in *Escherichia coli* and bacteriophage lambda. *Microbiol. Mol. Biol. Rev.* **63**, 751–813 (1999).
2. Kowalczykowski, S. C., Dixon, D. A., Eggleston, A. K., Lauder, S. D. & Rehrauer, W. M. Biochemistry of homologous recombination in *Escherichia coli*. *Microbiol. Rev.* **58**, 401–465 (1994).
3. Gelles, J. & Landick, R. RNA polymerase as a molecular motor. *Cell* **93**, 13–16 (1998).
4. Lovett, S. T., Luisi-DeLuca, C. & Kolodner, R. D. The genetic dependence of recombination in recD mutants of *Escherichia coli*. *Genetics* **120**, 37–45 (1988).
5. Schafer, D. A., Gelles, J., Sheetz, M. P. & Landick, R. Transcription by single molecules of RNA polymerase observed by light microscopy. *Nature* **352**, 444–448 (1991).
6. Yin, H., Landick, R. & Gelles, J. Tethered particle motion method for studying transcript elongation by a single RNA polymerase molecule. *Biophys J.* **67**, 2468–2478 (1994).
7. Finzi, L. & Gelles, J. Measurement of lactose repressor-mediated loop formation and breakdown in single DNA molecules. *Science* **267**, 378–380 (1995).
8. Roman, L. J. & Kowalczykowski, S. C. Characterization of the adenosinetriphosphatase activity of the *Escherichia coli* RecBCD enzyme: relationship of ATP hydrolysis to the unwinding of duplex DNA. *Biochemistry* **28**, 2873–2881 (1989).
9. Roman, L. J. & Kowalczykowski, S. C. Characterization of the helicase activity of the *Escherichia coli* RecBCD enzyme using a novel helicase assay. *Biochemistry* **28**, 2863–2873 (1989).
10. Okada, Y. & Hirokawa, N. A processive single-headed motor: kinesin superfamily protein KIF1A. *Science* **283**, 1152–1157 (1999).
11. Svoboda, K., Schmidt, C. F., Schnapp, B. J. & Block, S. M. Direct observation of kinesin stepping by optical trapping interferometry. *Nature* **365**, 721–727 (1993).
12. Guajardo, R. & Sousa, R. A model for the mechanism of polymerase translocation. *J. Mol. Biol.* **265**, 8-19 (1997).
13. Thaler, D. S. *et al.* in *Mechanisms and Consequences of DNA Damage Processing* (eds Friedberg, E. & Hanawalt, P.) 413–422 (Alan. R. Liss, New York, 1988).
14. Dixon, D. A., Churchill, J. J. & Kowalczykowski, S. C. Reversible inactivation of the *Escherichia coli* RecBCD enzyme by the recombination hotspot chi in vitro: evidence for functional inactivation or loss of the RecD subunit. *Proc. Natl Acad. Sci. USA* **91**, 2980–2984 (1994).
15. Myers, R. S., Kuzminov, A. & Stahl, F. W. The recombination hot spot chi activates RecBCD recombination by converting *Escherichia coli* to a recD mutant phenocopy. *Proc. Natl Acad. Sci. USA* **92**, 6244–6248 (1995).
16. Stahl, F. W., Thomason, L. C., Siddiqi, I. & Stahl, M. M. Further tests of a recombination model in which chi removes the RecD subunit from the RecBCD enzyme of *Escherichia coli*. *Genetics* **126**, 519–533 (1990); erratum *ibid.* **135**, 1232 (1993).
17. Taylor, A. F. & Smith, G. R. Regulation of homologous recombination: Chi inactivates RecBCD enzyme by disassembly of the three subunits. *Genes Dev.* **13**, 890–900 (1999).
18. Koppen, A., Krobitsch, S., Thoms, B. & Wackernagel, W. Interaction with the recombination hot spot chi in vivo converts the RecBCD enzyme of *Escherichia coli* into a chi-independent recombinase by inactivation of the RecD subunit. *Proc. Natl Acad. Sci. USA* **92**, 6249–6253 (1995).
19. Anderson, D. G., Churchill, J. J. & Kowalczykowski, S. C. Chi-activated RecBCD enzyme possesses 5′ —3′ nucleolytic activity, but RecBC enzyme does not: evidence suggesting that the alteration induced by Chi is not simply ejection of the RecD subunit. *Genes Cells* **2**, 117–128 (1997).
20. Dixon, D. A. & Kowalczykowski, S. C. The recombination hotspot chi is a regulatory sequence that acts by attenuating the nuclease activity of the *E. coli* RecBCD enzyme. *Cell* **73**, 87–96 (1993).
21. Roman, L. J., Eggleston, A. K. & Kowalczykowski, S. C. Processivity of the DNA helicase activity of *Escherichia coli* recBCD enzyme. *J. Biol. Chem.* **267**, 4207–4214 (1992).
22. Taylor, A. F., Schultz, D. W., Ponticelli, A. S. & Smith, G. R. RecBC enzyme nicking at Chi sites during DNA unwinding: location and orientation-dependence of the cutting. *Cell* **41**, 153–163 (1985).
23. Cronan, J. E. Jr Biotination of proteins in vivo. A post-translational modification to label, purify, and study proteins. *J. Biol. Chem.* **265**, 10327–10333 (1990).
24. Boehmer, P. E. & Emmerson, P. T. *Escherichia coli* RecBCD enzyme: inducible overproduction and reconstitution of the ATP-dependent deoxyribonuclease from purified subunits. *Gene* **102**, 1–6 (1991).
25. Eichler, D. C. & Lehman, I. R. On the role of ATP in phosphodiester bond hydrolysis catalyzed by the recBC deoxyribonuclease of *Escherichia coli*. *J. Biol. Chem.* **252**, 499–503 (1977).
26. Young, E. C., Berliner, E., Mahtani, H. K., Perez-Ramirez, B. & Gelles, J. Subunit interactions in dimeric kinesin heavy chain derivatives that lack the kinesin rod. *J. Biol. Chem.* **270**, 3926–3931 (1995).
27. Berliner, E. *et al.* Microtubule movement by a biotinated kinesin bound to streptavidin-coated surface. *J. Biol. Chem.* **269**, 8610–8615 (1994); erratum *ibid.* **269**, 23382 (1994).
28. Anderson, D. G., Churchill, J. J. & Kowalczykowski, S. C. A single mutation, RecB(D1080A) eliminates RecA protein loading but not Chi recognition by RecBCD enzyme. *J. Biol. Chem.* **274**, 27139–27144 (1999).
29. Berliner, E., Young, E. C., Anderson, K., Mahtani, H. K. & Gelles, J. Failure of a single-headed kinesin to track parallel to microtubule protofilaments. *Nature* **373**, 718–721 (1995).
30. Taylor, A. F. & Smith, G. R. Strand specificity of nicking of DNA at Chi sites by RecBCD enzyme. Modulation by ATP and magnesium levels. *J. Biol. Chem.* **270**, 24459–24467 (1995).

Supplementary information is available on *Nature*'s World-Wide Web site (http://www.nature.com).

Acknowledgements

We thank P. Bianco, P. Boehmer, S. Kowalczykowski, S. Lovett and A. Taylor for materials and helpful advice. This work was supported by the NIGMS.

Correspondence and requests for materials should be addressed to J.G. (e-mail: gelles@brandeis.edu).

Processive translocation and DNA unwinding by individual RecBCD enzyme molecules

Piero R. Bianco*†, Laurence R. Brewer‡, Michele Corzett§, Rod Balhorn§, Yin Yeh‖, Stephen C. Kowalczykowski*† & Ronald J. Baskin†

*Sections of * Microbiology and of † Molecular and Cellular Biology and ‖ Department of Applied Science, University of California at Davis, Davis, California 95616, USA*
‡ Electronics Engineering Technologies Division, and § Biology and Biotechnology Research Program, Lawrence Livermore National Laboratory, Livermore, California 94550, USA

RecBCD enzyme is a processive DNA helicase[1] and nuclease[2] that participates in the repair of chromosomal DNA through homologous recombination[3,4]. We have visualized directly the movement of individual RecBCD enzymes on single molecules of double-stranded DNA (dsDNA). Detection involves the optical trapping of solitary, fluorescently tagged dsDNA molecules that are attached to polystyrene beads, and their visualization by fluorescence microscopy[5,6]. Both helicase translocation and DNA unwinding are monitored by the displacement of fluorescent dye from the DNA by the enzyme[7]. Here we show that unwinding is both continuous and processive, occurring at a maximum rate of 972 ± 172 base pairs per second (0.30 μm s^{-1}), with as many as 42,300 base pairs of dsDNA unwound by a single RecBCD enzyme molecule. The mean behaviour of the individual RecBCD enzyme molecules corresponds to that observed in bulk solution.

Visualization of translocation and DNA unwinding by single DNA helicase molecules permits study of the stochastic properties of individual molecular motors, or 'nano-machines', which are obscured in the population average of steady-state, bulk-phase measurements. To achieve such visualization, we manipulated individual, fluorescently labelled DNA molecules by using an optical trap, and detected their unwinding by RecBCD enzyme. DNA substrates were constructed by attaching a biotinylated oligonucleotide to one cohesive end of lambda (λ) DNA. These DNA molecules were attached at low density to 1-μm streptavidin-coated, polystyrene beads. The fluorescent dye YOYO-1 was bound to the DNA, and then RecBCD enzyme was bound to these fluorescent DNA molecules in the absence of ATP. Under these conditions, RecBCD enzyme binds only to the free end of the dsDNA, and neither translocates nor unwinds the DNA until ATP is introduced[8].

These helicase–DNA complexes were introduced into one channel of a Y-shaped, micro-machined flow cell (Fig. 1a; and ref. 6). Helicase reaction buffer containing ATP was introduced into the second channel under conditions of laminar flow, creating a situation in

which the two solutions flowed parallel to one another with negligible mixing. The optically trapped bead appeared as a white sphere (the result of nonspecific binding of YOYO-1 to the bead), with an attached fluorescent DNA 'string' caused by flow-induced extension of the DNA molecule away from the trapped bead[5,6]. Once a RecBCD enzyme–DNA–bead complex was trapped, the stage was moved to reposition this complex, from the sample side of the flow cell across the flow boundary between solutions to the reaction side. If a RecBCD enzyme molecule is attached at the end opposite to the bead, then DNA unwinding will proceed from that end towards the bead, resulting in a decreased length of duplex DNA owing to concomitant unwinding of the dsDNA and displacement of YOYO-1 molecules by a single translocating RecBCD enzyme; the displaced free dye molecules possess negligible solution fluorescence (Fig. 1).

The observed unwinding of individual DNA molecules is shown in Fig. 2. Sequential video frames from representative reactions in the presence and absence of ATP are shown in Fig. 2a and b, respectively (see Supplementary Information). Before movement of the bead with the attached RecBCD–DNA complex to the reaction (ATP) side of the flow cell, the length of the DNA remains constant (first ~18 s of Fig. 2c). On relocation to the reaction side of the flow cell, a rapid decrease (0.145 $\mu m\,s^{-1}$) in the DNA length is observed when 1 mM ATP is present. DNA shortening is linear and constant, with no discernible pauses for a period of ~56 s, at which point the change in DNA length stops abruptly. (The occasional instantaneous deviation of DNA length from the average linear behaviour arises from movement of DNA slightly in and out of the focal plane; similar behaviour is observed for experiments either with or without ATP). The length remains constant for the remaining 42 s of this time course, suggesting that the cessation of unwinding results from dissociation of RecBCD enzyme from the remaining dsDNA.

The observed rate of DNA shortening (from $t = 18$ s to $t = 74$ s) corresponds to an apparent rate of DNA helicase movement of 471 ± 30 base pairs (bp) s^{-1} (see Methods). The change in length of dsDNA that occurs before RecBCD enzyme dissociates, 8.3 μm, corresponds to 26,800 ± 700 bp unwound by the single RecBCD enzyme. In contrast, in the absence of ATP there is only a small decrease in the apparent length of the DNA (~ 1 μm) at a rate that is 16-fold lower than the ATP-dependent reaction (−0.009 $\mu m\,s^{-1}$ versus −0.145 $\mu m\,s^{-1}$). This change in apparent length is enzyme-independent, and results from a slow dissociation of YOYO-1 from sites across the entire length of the DNA molecule that occurs when the DNA molecule is relocated from the sample to the reaction side of the flow cell, owing to the lower YOYO-1 concentration on the reaction side (Fig. 2b; and data not shown). Control experiments done in the presence of ATP, but in the absence of enzyme, produced results identical to those obtained in the absence of ATP (data not shown) and showed that, at longer times, a new equilibrium DNA length was achieved (YOYO-1 elongates dsDNA by 1.1–1.2-fold; refs 5, 6, 9). When the unwinding rate in the presence of 1 mM ATP is corrected for the enzyme-free dissociation of YOYO-1, the corrected unwinding rate (k_{cat}^{corr}) is 443 ± 30 bp s^{-1}. We conclude that this unwinding rate is due to a single molecule of RecBCD enzyme that bound to the free dsDNA end opposite the bead, and both translocated and unwound the DNA in an ATP-dependent manner once the DNA entered the ATP channel. Additional RecBCD enzyme molecules could not have contributed to the unwinding because RecBCD enzyme binds only to blunt, or nearly blunt dsDNA ends, with a greater than 1 million-fold preference relative to internal sites[10,11], and RecBCD enzyme was present only in the sample side of the flow cell.

To confirm further that the unwinding observed was dependent on RecBCD enzyme, we carried out assays at four additional ATP concentrations and also at 37 °C, because previous steady-state kinetic assays showed that the rate of unwinding depends on both of these variables[11,12]. As expected, the observed rate of unwinding increased with increasing ATP concentration (Fig. 3). In all cases,

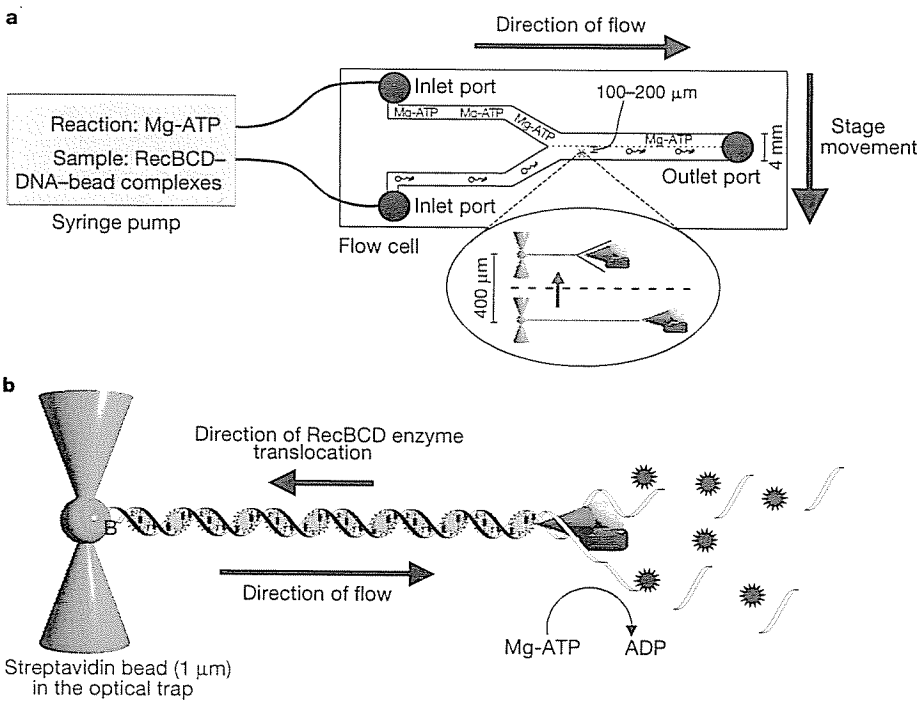

Figure 1 Visualization of DNA helicase action on individual DNA molecules. **a**, Syringe pump and flow cell: the sample syringe contains helicase–DNA–bead complexes, and the reaction syringe contains ATP. 'X' indicates the laser trap position, and the red arrow indicates movement of the trapped DNA–bead complex across the boundary between solutions. Inset, the trapped DNA with bound helicase, and its unwinding after relocation into the reaction solution. **b**, Fluorescent DNA helicase assay[7]. A trapped and stretched, fluorescent DNA molecule is shown. As RecBCD enzyme translocates, it both unwinds and degrades the DNA, simultaneously displacing dye molecules (black stars). B, biotinylated oligonucleotide.

unwinding of dsDNA molecules was continuous and without any detectable pausing, indicating that the helicase action of individual RecBCD enzymes was not affected detectably by any sequence present in the λ DNA. Microscopic pausing, at the individual base-pair level, would not be detected in our experiments because this is beyond the temporal (33 ms per frame; hence pauses shorter than about 10 frames, or ~330 ms, would be difficult to detect) and spatial resolution of the assay system (a maximum of ~244 nm or 800 bp but, owing to occasional movement of the DNA out of the focal plane, the actual resolution is lower, ~1 μm or ~3,000 bp). Hence, there is no class of limited (10–20) specific pause sites at which the enzyme pauses for more than a fraction of a second or so.

Although the rate of DNA unwinding by any individual RecBCD enzyme molecule was uniform (within experimental error) on any given DNA molecule (Fig. 2), the rate for different helicase molecules deviated by 1.4–5-fold at each ATP concentration examined (Fig. 3). However, their average behaviour at each ATP concentration was similar to that observed in both steady-state solution experiments[1,11] and electron microscopic assays that analysed intermediates of the unwinding reaction[13]. For example, at 250 μM ATP

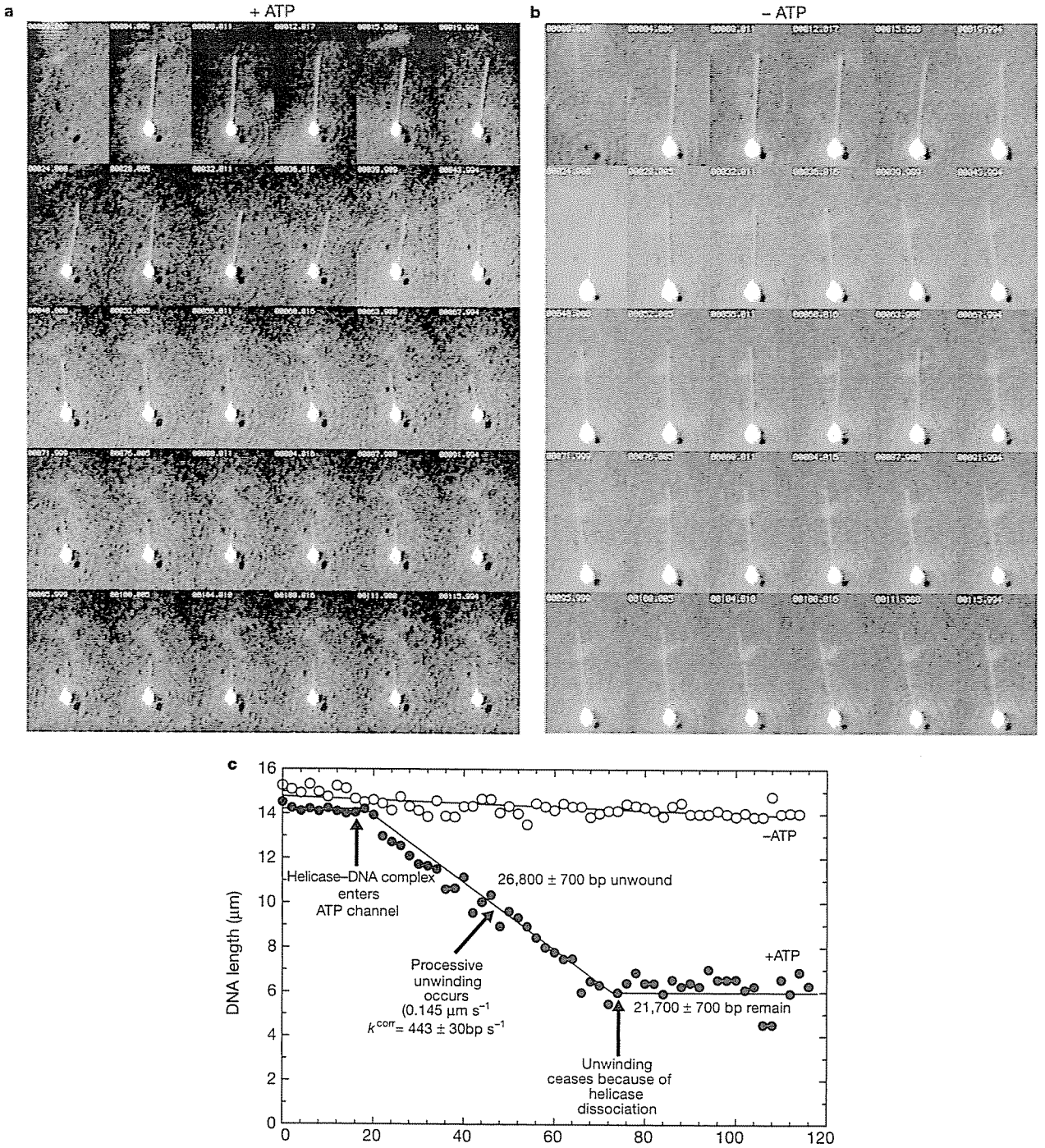

Figure 2 Unwinding of a DNA molecule by RecBCD enzyme. **a**, **b**, Selected, sequential frames from a video recording of reactions either in the presence (**a**) or absence (**b**) of ATP (1 mM). The direction of translocation and DNA unwinding by RecBCD enzyme is from the DNA end opposite the bead, towards the bead (that is, from the top of each frame towards the bottom). Numbers at the top of each frame indicate elapsed time. **c**, Analysis of the time courses in **a** and **b**.

the unwinding rate for eight individual enzymes varied from a minimum of 156 bp s^{-1} to a maximum of 428 bp s^{-1}, with an average of 359 ± 89 bp s^{-1}. A similar behaviour was observed at each of the four additional ATP concentrations used. Both this variation in unwinding rate by individual helicase molecules and the unfaltering movement could not have been discerned from steady-state experiments. At present, the source of this variation is unknown; some of the variation might be day-to-day variation or variation in the DNA–bead preparation used, but at least a twofold variance was observed for six molecules on the same day with the same DNA–bead preparation. Variation in individual enzymatic activity was observed for at least two other enzymes: lactate dehydrogenase[14] and T7 DNA polymerase[15]. Despite the individual variation, when the averaged data from the unwinding of 42 DNA molecules (Fig. 3a) were fitted to the Michaelis–Menten equation, a V_{max} of 521 ± 60 bp s^{-1} and a K_m^{ATP} of 142 ± 58 μM was obtained. Both values are virtually identical to those reported from bulk-solution experiments (586 ± 45 bp s^{-1} and 130 ± 30 μM ATP, respectively[11,12,16]). In addition to being dependent on ATP concentration, the rate of unwinding in 1 mM ATP increased twofold when the temperature was raised to 37 °C (Table 1); this k_{cat}^{corr} (972 ± 172 bp s^{-1}) is essentially identical to that obtained from steady-state measurements (930 ± 15 bp s^{-1}; ref. 11).

In addition to obtaining dsDNA unwinding rates, we directly observed the distance travelled by an individual RecBCD enzyme from its binding site at a dsDNA end to its point of dissociation, a distance that directly defines the processivity of DNA unwinding (that is, the number of base pairs unwound by a single helicase molecule per DNA binding event before dissociation) (Fig. 3b and Table 1). The processivity varied in an ATP-dependent fashion, with the maximum value observed at 1 mM ATP. There was a stochastic variation in the processivity of individual RecBCD enzyme molecules at any given ATP concentration (Fig. 3b). For example, at 250 μM ATP, unwinding terminated abruptly after values ranging from 9,200 to 39,500 bp of dsDNA unwound by eight different RecBCD enzymes. The average value is 22,900 ± 9,500 bp, which is similar to that determined previously (27,000 ± 3,000 bp; ref. 1).

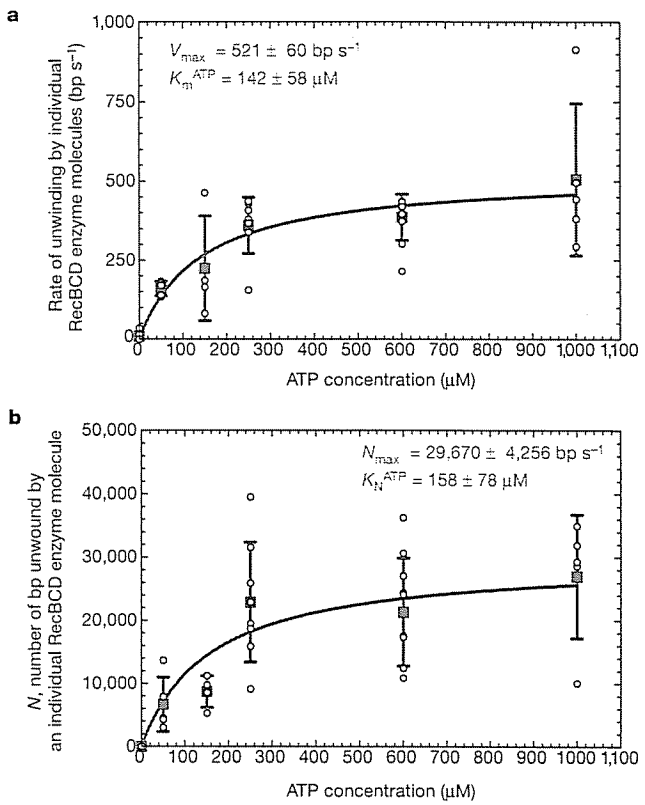

Figure 3 Both the rate and processivity for dsDNA unwinding by individual RecBCD enzyme molecules may vary, but their averages fall within ranges observed for bulk solution. For each ATP concentration (23 °C), 4–10 DNA molecules were measured on different days, using several different preparations. **a**, Unwinding rates for single RecBCD enzyme molecules; **b**, processivities for the same molecules. Open circles represent individual molecule results, and squares represent their average for a given ATP concentration (error bars indicate the standard deviation). Data were fitted to a hyperbola (red line) for comparison with previously published steady-state values[1].

Table 1 Summary of DNA helicase behaviour for individual RecBCD enzymes

Temperature (°C)	ATP concentration (mM)	$k_{cat}^{corr.}$ (bp s^{-1} per RecBCD)*	N (bp per end)†
23	0.05	161 ± 23 (5)‡	6,700 ± 4,300
23	0.15	224 ± 166 (4)	9,600 ± 3,000
23	0.25	359 ± 89 (8)	22,900 ± 9,500
23	0.60	386 ± 71 (10)	21,300 ± 8,500
23	1.00	502 ± 243 (5)	27,000 ± 9,800
37	1.00	972 ± 172 (3)	38,000 ± 5,700

* The observed unwinding rate as calculated for the linear portion of plots such as those shown in Fig. 2c. As the rate is determined from an individual enzyme molecule, we refer to it as k_{cat}; it has been corrected for the ATP-independent rate, thus k_{cat}^{corr}. The observed variation is the standard deviation of unwinding rates for individual RecBCD enzyme molecules at that ATP concentration.
† N is the number of base pairs of dsDNA translocated and unwound by an individual RecBCD enzyme molecule. The reported variation is the standard deviation of the processivity for all enzyme molecules at a particular ATP concentration.
‡ The number in parentheses indicates the number of DNA molecules used to determine the unwinding rates and the processivities at each ATP concentration; eight molecules were examined in the absence of ATP.

We fitted the processivity data from the same 40 molecules analysed in Fig. 3a to a hyperbolic function to determine a maximum processivity at 23 °C of 29,670 ± 4,256 bp per binding event, with an apparent K_m^{ATP} for processive unwinding (K_N^{ATP}) of 158 ± 78 μM (Fig. 3b; and ref. 1). These results are similar to those reported previously for RecBCD enzyme using both gel and fluorescence measurements (32,000 ± 1,800 bp per end, and K_N^{ATP} = 41 ± 9 μM; ref. 1). The processivity is even higher at elevated temperature, increasing to an average of 38,000 ± 5,700 bp per dsDNA end-binding event (Table 1); in fact one RecBCD enzyme molecule could unwind as much as 42,300 bp of dsDNA. As the translocation step size is 23 bp (ref. 17), a single RecBCD enzyme has the capacity to take as many as 1,840 steps (translocating a total distance of 13 μm) before dissociating when the ATP concentration is not limiting.

We have observed both the rate and processivity of dsDNA unwinding for individual RecBCD enzyme molecules using a single-molecule helicase assay. To our knowledge, this is the first time that the action of individual DNA helicase molecules on dsDNA substrates has been observed in real time. The results obtained are consistent with and in precise agreement with previously published reports[1,11,7,12]. This assay has further potential and can be used to study a variety of individual nucleic acid enzymes: both those that simply bind to nucleic acids to effect a conformational change (for example, the DNA strand-exchange protein, RecA protein, that displaces fluorescent dye molecules upon binding to dsDNA[18]), and those that process DNA in a manner similar to that observed here. □

Methods

Optical trapping and fluorescence microscopy

DNA helicase reactions were performed in a two-channel, Y-shaped, micro-machined glass flow cell[6] (Fig. 1) with the inlet ports connected to 1-ml syringes controlled by a syringe pump (Model KDS 200; KD Scientific, Boston, MA). The flow cell was held in place on a motorized stage controlled by an MSI-2000 computerized stage controller (0.1-μm resolution; Applied Scientific Instruments). The stage was positioned in a Nikon ES400 microscope, which was equipped for epifluorescence and modified to incorporate an optical trap. The optical trap used an Nd:YLF infrared laser (wavelength 1,047 nm, 500 mW; Spectra Physics) focused through an oil-immersion objective lens (Plan Fluor 100×, 1.3 N.A.; Nikon) and Immersol (518F, low fluorescence; a gift from Zeiss), to a position 10–15 μm below the upper surface of the flow cell. The flow cell is ~4,000 μm wide, and trapping is initially done 100–200 μm from the boundary between solutions on the sample side of the flow cell, to ensure that a trapped complex that may have a RecBCD enzyme molecule attached, has not been exposed to ATP. The trapped complex is moved

~400 μm into the reaction side to ensure that the reaction occurs in a homogenous concentration of ATP.

Fluorescent DNA–bead complexes were excited with the microscope's high-pressure mercury lamp using the appropriate filter set (blue filter set #11001; Chroma Technology, Brattleboro, VT). Fluorescence images were captured by a charge-coupled device camera (CCD-300T-IGF; Dage-MTI, Michigan City, IN) coupled to an image intensifier (VS4-1845; Video-Scope International, Sterling, VA), and were recorded on VHS videotape. To increase temperature to 37 °C, the microscope stage was enclosed in a Plexiglas housing and warm air was introduced.

DNA–bead preparation

The protocol used was modified from ref. 6. Bacteriophage λ DNA (0.096 pmoles; New England Biolabs) was biotinylated at one end by annealing and ligating a 3′-biotinylated, 12-mer oligonucleotide (50 pmoles; Operon Technologies) complementary to one of the cohesive ends. The biotinylated λ DNA ($3.6–7.2 \times 10^8$ molecules total) was reacted with 1 μm, streptavidin-coated, polystyrene beads (1.92×10^8 beads total; Bangs Laboratories) in 82 mM $NaHCO_3$ (pH 8.0) at 37 °C for 60 min. DNA–bead complexes were immediately transferred to a degassed solution containing 57 mM $NaHCO_3$ (pH 8.0), 30 mM dithiothreitol (DTT), 20% sucrose and 0.2 μM YOYO-1 (Molecular Probes). Dye binding was performed for a minimum of 60 min at 24 °C in the dark.

Single-molecule DNA helicase reactions

Before use, the flow cell was coated with either casein or BSA (100 $\mu g\,ml^{-1}$). The excess, unbound protein was washed out using 100 mM $NaHCO_3$ (pH 8.0). For each assay the sample syringe contained 41 mM $NaHCO_3$ buffer (pH 8.0), 35 mM DTT, 13% sucrose, 0.133 μM YOYO-1, 2 mM magnesium acetate, 1.92×10^8 DNA–bead complexes, and 4.6 nM RecBCD enzyme. The reaction syringe contained 41 mM $NaHCO_3$ buffer (pH 8.0), 35 mM DTT, 13% sucrose, 0.02 μM YOYO-1, 2 mM magnesium acetate, and ATP at the correct concentration. The *Escherichia coli* single-stranded DNA (ssDNA)-binding protein was not needed in these reactions because endonucleolytic cleavage of unwound ssDNA by the associated nuclease activity of RecBCD enzyme, releases the ssDNA as fragments that are immediately washed away in the buffer flow and, thus, do not accumulate to either inhibit the enzyme[19] or affect the observed fluorescence signal[7].

The RecBCD enzyme preparation used in all experiments was 100% active (data not shown) as determined using a spectrofluorometric helicase assay[11]. Standard visualization reactions were done at room temperature (~23 °C) using degassed buffers. Flow was initially at 0.8 $ml\,h^{-1}$ for 10 min and was gradually decreased in increments of 50% to a final flow rate 10–20 $\mu l\,h^{-1}$ (linear flow rates of ~80–150 $\mu m\,s^{-1}$), over a period of ~20 min.

Data analysis

Images were captured on a Power PC Macintosh computer interfaced with the VCR through an LG-3 frame-grabber card, operating at 1 frame per 33 ms, and controlled by Scion NIH Image v1.62c (Scion Corporation). Captured videos were converted into individual, time-stamped, sequential frames (Fig. 2) to make measurements. Individual DNA molecules were measured using the linear measurement tool of Scion NIH Image; calibration of the microscope optics was achieved using an Objective Micrometer (Fisher Scientific) that was marked in units of 10 μm.

The rate of DNA unwinding was calculated by measuring the observed length of DNA in each frame of a time course and fitting the resultant data to a linear function by least squares analysis. The resulting slope in each ATP-dependent reaction was corrected using the slope determined in the absence of ATP; this corrected slope was multiplied by the number of bp of λ DNA per μm to calculate the corrected rate in units of bp s^{-1}. Under the assay conditions used, the average length of individual, stretched, fluorescent λ DNA molecules was 14.9 μm ($n = 43$), which is shorter than previously published lengths[5,6]. Those reports used a higher concentration of sucrose and were done in the absence of magnesium ions. In our experiments, the length of a single, stretched λ DNA molecule was affected by flow rate and by the concentrations of sucrose, magnesium ions, and YOYO-1, varying from nore than 18 μm in 20% sucrose in the absence of magnesium acetate, to 14.9 μm in 13% sucrose and 2 mM magnesium acetate (data not shown). Thus, for all calculations, as λ DNA is 48,502 bp in length, and the observed average length of a λ DNA molecule is 14.9 μm, the average number of bp per μm is 48,502/14.9 = 3,255.

Received 23 May; accepted 23 October 2000.

1. Roman, L. J., Eggleston, A. K. & Kowalczykowski, S. C. Processivity of the DNA helicase activity of *Escherichia coli* recBCD enzyme. *J. Biol. Chem.* **267,** 4207–4214 (1992).
2. Arnold, D. A. & Kowalczykowski, S. C. in *Encyclopedia of Life Sciences* [online] (Nature Publishing Group, London, 1999) (http://www.els.net).
3. Kowalczykowski, S. C., Dixon, D. A., Eggleston, A. K., Lauder, S. D. & Rehrauer, W. M. Biochemistry of homologous recombination in *Escherichia coli*. *Microbiol. Rev.* **58,** 401–465 (1994).
4. Kuzminov, A. Recombinational repair of DNA damage in *Escherichia coli* and bacteriophage lambda. *Microbiol. Mol. Biol. Rev.* **63,** 751–813 (1999).
5. Perkins, T. T., Smith, D. E. & Chu, S. Direct observation of tube-like motion of a single polymer chain. *Science* **264,** 819–822 (1994).
6. Brewer, L. R., Corzett, M. & Balhorn, R. Protamine-induced condensation and decondensation of the same DNA molecule. *Science* **286,** 120–123 (1999).
7. Eggleston, A. K., Rahim, N. A. & Kowalczykowski, S. C. A helicase assay based on the displacement of fluorescent, nucleic acid-binding ligands. *Nucleic Acids Res.* **24,** 1179–1186 (1996).
8. Ganesan, S. & Smith, G. R. Strand-specific binding to duplex DNA ends by the subunits of *Escherichia coli* recBCD enzyme. *J. Mol. Biol.* **229,** 67–78 (1993).
9. Bennink, M. L. *et al.* Single-molecule manipulation of double-stranded DNA using optical tweezers: interaction studies of DNA with RecA and YOYO-1. *Cytometry* **36,** 200–208 (1999).
10. Taylor, A. F. & Smith, G. R. Substrate specificity of the DNA unwinding activity of the RecBC enzyme of *Escherichia coli*. *J. Mol. Biol.* **185,** 431–443 (1985).
11. Roman, L. J. & Kowalczykowski, S. C. Characterization of the helicase activity of the *Escherichia coli* RecBCD enzyme using a novel helicase assay. *Biochemistry* **28,** 2863–2873 (1989).
12. Eggleston, A. K. & Kowalczykowski, S. C. The mutant recBCD enzyme, $recB^{2109}$CD enzyme, has helicase activity but does not promote efficient joint molecule formation *in vitro*. *J. Mol. Biol.* **231,** 621–633 (1993).
13. Taylor, A. & Smith, G. R. Unwinding and rewinding of DNA by the recBC enzyme. *Cell* **22,** 447–457 (1980).
14. Xue, Q. F. & Yeung, E. S. Differences in the chemical reactivity of individual molecules of an enzyme. *Nature* **373,** 681–683 (1995).
15. Wuite, G. J. L., Smith, S. B., Young, M., Keller, D. & Bustamante, C. Single-molecule studies of the effect of template tension on T7 DNA polymerase activity. *Nature* **404,** 103–106 (2000).
16. Roman, L. J. & Kowalczykowski, S. C. Characterization of the adenosinetriphosphatase activity of the *Escherichia coli* RecBCD enzyme: Relationship of ATP hydrolysis to the unwinding of duplex DNA. *Biochemistry* **28,** 2873–2881 (1989).
17. Bianco, P. R. & Kowalczykowski, S. C. Step size measurements on the translocation mechanism of the RecBC DNA helicase. *Nature* **405,** 368–372 (2000).
18. Zaitsev, E. N. & Kowalczykowski, S. C. Binding of double-stranded DNA by *Escherichia coli* RecA protein monitored by a fluorescent dye displacement assay. *Nucleic Acids Res.* **26,** 650–654 (1998).
19. Anderson, D. G. & Kowalczykowski, S. C. SSB protein controls RecBCD enzyme nuclease activity during unwinding: a new role for looped intermediates. *J. Mol. Biol.* **282,** 275–285 (1998).

Supplementary information is available on *Nature*'s World-Wide Web site (http://www.nature.com) or as paper copy from the London editorial office of *Nature*.

Acknowledgements

We would like to thank S. Chan and J. Lengyel for assistance with measurements, and the following people for their comments on the manuscript: N. Handa, J. Kleiman, A. Mazin, J. New, E. Seitz, M. Spies, T. Sugiyama and Y. Wu. This work was supported by an NIH Grant to S.C.K. and a DOE Center of Excellence for Laser Applications in Medicine Grant to Y.Y. and R.J.B.

Correspondence and requests for materials should be addressed to S.C.K. (e-mail: sckowalczykowski@ucdavis.edu).

Crystal structure of the transcription activator BmrR bound to DNA and a drug

Ekaterina E. Zheleznova Heldwein & Richard G. Brennan

Department of Biochemistry and Molecular Biology, Oregon Health Sciences University, Portland, Oregon 97201-3098, USA

The efflux of chemically diverse drugs by multidrug transporters that span the membrane[1] is one mechanism of multidrug resistance in bacteria. The concentrations of many of these transporters are controlled by transcription regulators, such as BmrR in *Bacillus subtilis*[2], EmrR in *Escherichia coli*[3] and QacR in *Staphylococcus aureus*[4]. These proteins promote transporter gene expression when they bind toxic compounds. BmrR activates transcription of the multidrug transporter gene, *bmr*, in response to cellular invasion by certain lipophilic cationic compounds (drugs)[2,5,6]. BmrR belongs to the MerR family, which regulates response to stress such as exposure to toxic compounds or oxygen radicals in bacteria[7–12]. MerR proteins have homologous amino-terminal DNA-binding domains but different carboxy-terminal domains, which enable them to bind specific 'coactivator' molecules. When bound to coactivator, MerR proteins upregulate transcription by reconfiguring the 19-base-pair spacer found between the –35 and –10 promoter elements to allow productive interaction with RNA polymerase[7,9–12]. Here we report the 3.0 Å resolution structure of BmrR in complex with the drug tetraphenylphosphonium (TPP) and a 22-base-pair oligodeoxynucleotide encompassing the *bmr* promoter. The structure reveals an unexpected mechanism for transcription activation that involves localized base-pair breaking, and base sliding and realignment of the –35 and –10 operator elements.

THE JOURNAL OF BIOLOGICAL CHEMISTRY

Vol. 277, No. 41, Issue of October 11, pp. 38895–38900, 2002
Printed in U.S.A.

Condensation of DNA by Spermatid Basic Nuclear Proteins*

Received for publication, May 15, 2002, and in revised form, July 17, 2002
Published, JBC Papers in Press, July 24, 2002, DOI 10.1074/jbc.M204755200

Laurence Brewer‡§, Michele Corzett¶, and Rod Balhorn¶

From the ‡Electronics Engineering Technologies Division and ¶Biology and Biotechnology Research Program, Lawrence Livermore National Laboratory, Livermore, California 94550

Two transition proteins, TP1 and TP2, participate in the repackaging of the spermatid genome early in mammalian spermiogenesis, coincident with the first detectable changes in chromatin condensation. Using an optical trap and a two-channel flow cell to move single DNA molecules into buffer containing protein, we have measured the rates of DNA condensation and decondensation induced by the binding of Syrian hamster transition proteins TP1 and TP2 and protamines P1 and P2. The results show that both transition proteins condense free DNA, with rates similar to those of protamine 1 and 2. DNA molecules condensed with TP1 were significantly less stable than DNA condensed by protamine or by TP2. Experiments conducted with a peptide corresponding to the C-terminal 25 residues of TP2 showed that this domain is responsible for condensing DNA. Experiments conducted with two fragments of TP1 containing arginine and lysine residues demonstrated that DNA binding by TP1 must involve more than these basic sequences. Zinc facilitated the condensation of DNA by P2 but not by TP2. The dissociation rates of TP2 and P2 from DNA were not affected by the addition of zinc.

The structure of chromatin is changed dramatically during the final stages of spermiogenesis in mammals as the spermatid's genome is condensed and inactivated by the sequential binding of several basic nuclear proteins (1). Although the most dramatic change in condensation occurs in late-step spermatids (2) when the protamines displace transition proteins TP1 and TP2 (3) and coil the DNA into toroidal subunits (4), the replacement of histones by these two transition proteins several days earlier coincides with the first appearance of a detectable change in the condensation state of chromatin (5, 6). Studies in the rat have demonstrated that the deposition of the two transition proteins in spermatid chromatin occurs sequentially, with TP2 appearing first in step 10 spermatids. TP1 was observed to appear ~24 h later in step 12 spermatids (7).

Previous experiments have shown that TP2 binds preferentially to CG sequences, and the observation that TP2 appears early in spermatid chromatin (8) suggested that the function of TP2 may be to shut down transcription by binding to the CG islands that are associated with gene promoter domains. TP1, which appears a day later, has been reported to stimulate DNA repair of single-stranded breaks (9) and is suggested to function by binding to the breaks induced during the removal of the histones until they can be repaired (9, 10). Following the removal of the histones and the repair or ligation of the single-stranded breaks, protamines are synthesized and deposited on chromatin to complete the compaction of the chromatin and ensure the sperm genome remains inactive until it can be deposited inside an egg and reactivated.

Protamines, on the other hand, are highly charged, arginine-rich proteins that bind to DNA in a nonspecific manner. Previous *in vivo* and *in vitro* studies have been carried out to determine how DNA is condensed by protamines. The primary factor that induces compaction is thought to be the neutralization of the negative charge on the phosphodiester backbone of DNA, which is achieved when protamines bind (11, 12). The condensation of duplex DNA by protamine occurs in a unique fashion, one that involves the coiling of the sperm's DNA into toroidal subunits containing ~50 kb of DNA (4, 13, 14). Similar structures have been produced *in vitro* using a variety of polycations (15–17) including protamine (13, 18). At the completion of spermatid maturation, the mature sperm cell has been estimated to contain as many as 50,000 of these toroidal structures packed inside the nucleus (4).

Several studies performed *in vitro* have shown that both TP1 and TP2 bind to and condense DNA (8, 9, 19–22), but the mechanism of condensation (DNA collapse, intermolecular aggregation, toroid formation) has not been resolved. Previous experiments have suggested that TP2 is more effective in condensing DNA than TP1 (20). Analyses of the TP2 protein sequence (23) (Table I) and DNA-binding experiments conducted with fragments of the TP2 protein (21) have also provided evidence to suggest that the TP2 protein may have two structural domains, an amino-terminal sequence that provides the protein with a specificity for binding to CG islands (8) and a carboxyl-terminal arginine- and lysine-rich segment that enhances the protein's ability to condense DNA. TP1 contains three short arginine- and lysine-rich sequences of 4–5 residues each, which may participate in its binding to DNA (23).

Using a new technique that permits the analysis of the kinetics of DNA condensation without the complications of intermolecular aggregation, we have examined TP1- and TP2-mediated DNA condensation to determine whether these proteins are capable of inducing the condensation of single, histone-free DNA molecules *in vitro*. The results show that the condensation rates observed for TP1 and TP2 are similar to those obtained with protamines 1 and 2. Experiments were also conducted to assess the stability of the protamine and transition protein-DNA complexes and determine whether particular basic segments of the proteins bind and participate in DNA condensation. The effect of zinc on the condensation/dissociation process induced by these transition proteins and protamines was also investigated.

* This work was performed under the auspices of the United States Department of Energy by the University of California Lawrence Livermore National Laboratory under Contract W-7405-ENG-48. The costs of publication of this article were defrayed in part by the payment of page charges. This article must therefore be hereby marked "*advertisement*" in accordance with 18 U.S.C. Section 1734 solely to indicate this fact.

§ Supported by a grant from the NICHD, National Institutes of Health (1 K25 HD01387-02). To whom correspondence should be addressed. Tel.: 925-423-2343; Fax: 925-422-2373; E-mail: brewer1@llnl.gov.

TABLE I
Amino acid sequences for hamster protamines and mouse transition proteins
The positions of the synthesized TP1 and TP2 fragments are shown by underlining.

TP2 (mouse)	MDTKMQSLPTTHPHPHSSSRPQSHTSNQCNQCTCSHHCRSCSQAGHAGSSSSP
	SPGPPMKHPKPSVHSRHSPARPSHRGSCPKNRKTFEGKVSKRKAVRRRKRTHRAKRRTSGRRYK
TP1 (mouse)	STSRKLKTHGMRRGKNRAPHKGVKRGGSKRKYRKSVLKSRKRGDDASRNYRSHL
Protamine 2 (Syrian hamster)	MVRYRMRSPSERPHQGPGQEHGREEQQGQGQGLSPERVEDYGRTHRGQHHHRRRCS
	RRKLYRIHRRRRSCRRRRRHSCRHRRRHRRGCRRSRRRRRCRCRRCRRHHH
Protamine 1 (Syrian hamster)	ARYRCCRSKSRSRCRRRRRRCRRRRRRCCRRRRRRCCRRRRTYTLRCKRY

EXPERIMENTAL PROCEDURES

Isolation and Purification of Protamines and Transition Proteins—Hamster sperm were obtained by teasing the epididymides from sexually mature Syrian (*Mesocricetus auratus*) hamsters in Tris-saline and filtering the suspended sperm through 80-μm nylon gauze. The sperm basic nuclear proteins were extracted, and the two protamines were separated as described by Corzett *et al.* (24).

The transition proteins TP1 and TP2 were extracted from testicular spermatids. Frozen Syrian hamster testes were thawed, homogenized in a Virtis homogenizer at 5000 rpm for 3 min in 0.25 M sucrose, 0.01 M Tris, pH 8, 2.5 mM magnesium chloride, and 1 mM phenylmethylsulfonyl fluoride and filtered through three layers of cheese cloth. The nuclei were centrifuged at 4100 × *g* for 3 min at 4 °C. To remove contaminating somatic nuclei and early spermatids that were not sonication-resistant, the nuclear pellet was washed four times by sonicating it in distilled water with 1 mM phenylmethylsulfonyl fluoride and centrifuging the suspension at 3000 × *g* for 3 min (3). The sonication-resistant nuclear pellet was resuspended in 0.25 N HCl, 1 mM phenylmethylsulfonyl fluoride, and the proteins were extracted on ice for 1 h with occasional mixing and centrifuged at 10,500 × *g* for 10 min. The pellet was re-extracted for an additional hour, and the supernatants were pooled. Trichloroacteic acid was added to a final concentration of 3.5% for 1 h and then centrifuged at 4100 × *g* for 15 min to remove the protamines. Additional trichloroacteic acid was added to the supernatant to increase the concentration to 25% to precipitate the transition proteins. The precipitated proteins were sedimented by centrifugation, washed with acidified acetone, and air-dried.[1]

Protamines P1 and P2 and transition proteins TP1 and TP2 were separated and purified by high performance liquid chromatography (HPLC).[2] The extracted proteins were reduced with 30 mM dithiothreitol (DTT) in 3 M guanidine hydrochloride, 50 mM Tris, pH 8, for 1 h and were separated on a Hamilton PRP-1 column (200 × 7 mm, 5-μm particle size) using a linear acetonitrile gradient (20–32% buffer B at a flow rate of 2 ml/min over 20 min; buffer A = 0.1% trifluoroacetic acid; buffer B = 60% acetonitrile, 0.1% trifluoroacetic acid). Protein elution was monitored at 214 nm. Protein purity was determined by gel electrophoresis (protamines were aminoethylated with aziridine (25) prior to electrophoresis). Microdensitometric scans of the gels showed TP1, TP2, P1, and P2 were enriched to >95% purity.

The protein sequences of the two hamster protamines have been reported previously (24). However, neither the protein nor gene sequences for the Syrian hamster transition proteins TP1 and TP2 have been described in the literature. The amino acid compositions obtained for the hamster transition proteins (data not shown) confirmed their sequences are similar to their rat and mouse homologs (Table I) (23, 26–30).

Peptide Synthesis and Purification—Three peptides corresponding to basic regions of the TP1 and TP2 mouse transition proteins (23) were synthesized and purified by HPLC by SynPep Corp. (Dublin, CA). The two TP1 peptides, KRKYRKSVLKSRKR and RRGKNR, were synthesized with an acetylated amino terminus and amide on the carboxyl terminus to create peptides that more accurately mimic the corresponding internal peptide sequences present in TP1. The carboxyl terminus was left unmodified in the TP2 peptide, SKRKAVRRRKRTHRAKRRSSGRRYK, and its amino terminus was acetylated to eliminate the charge on the α-amino group in the peptide.

Protein Quantitation—To obtain accurate values for the concentrations of the nuclear proteins used in the condensation experiments, the purified proteins were dissolved in water, known aliquots were distributed into disposable glass tubes, and the samples were lyophilized. Replicate tubes were analyzed for their amino acid content by AAA Service Laboratory (Boring, OR). The protein content of each sample was determined using the known sequence of the protamines and the amino acid compositions of the rat and mouse TP1 and TP2 proteins predicted from their gene sequences. Tube to tube variation in the aliquoted samples used for the experimental studies were found to be less than 2%.

Preparation of Stained DNA Molecules Attached to Beads—Lambda phage DNA (Invitrogen) was tagged with biotin and attached to 1-μm diameter streptavidin-coated polystyrene beads (Bangs Laboratories Inc, Fishers, IN) as described previously (31). The DNA attached to beads was diluted in degassed 50% sucrose (w/v), 100 mM sodium bicarbonate pH 8, 30 mM DTT, and a sufficient quantity of YOYO-1 dye such that the dye molecule to DNA base pair ratio was less than or equal to 1:4. The same buffer, minus the YOYO-1 dye, was used for dissolving the protein samples. For experiments testing the effect of zinc (50 μM zinc chloride) on DNA condensation/decondensation, the antioxidant in the buffer used for both DNA and protein was changed from 30 mM DTT (which binds zinc) to 30 mM cysteamine.

Design of Condensation/Decondensation Experiments—The experimental apparatus (shown in Fig. 1*A*) is identical to that used previously to examine the condensation of individual DNA molecules by salmine (31, 32). Separate solutions of DNA molecules attached to polystyrene beads and protein were introduced into a dual-port flow cell (Fig. 1*A*) at a flow velocity of ~50 μm/s. Beads containing individual DNA molecules were trapped using an infrared laser optical trap and transported into the protein solution, where the condensation of an extended, single DNA molecule (Figs. 1*B* and 2) could be observed via fluorescence microscopy. An argon-ion laser (λ = 488 nm) was used to illuminate the YOYO-1 stained DNA molecules, which could be observed for times as long as 10–15 min before photobleaching occurred. The same molecule could then be observed as it decondensed by pulling the molecule back to the DNA side of the flow cell, where there was an absence of peptide, and watching the DNA molecule re-extend.

The fluorescence image of each DNA molecule was detected using an image-intensified CCD camera, and a frame grabber was used to digitize the resultant images. The conversion factor for the observed DNA length in μm to kb (2.53 kb/μm) was determined by measuring the length of stained lambda phage DNA (48.5 kb) extended by flow. It was measured to be 19.2 ± 0. 82 μm at a flow rate of 72 μm/s in 50% sucrose. Under these conditions the DNA was 95% extended.[3]

RESULTS

Previous experiments have shown that both salmine and bull protamine 1 induce the coiling and condensation of DNA molecules (31–33) into toroidal structures similar to those observed in native sperm chromatin (4). Single molecule fluorescence experiments (31) showed that condensation of DNA into a toroid appears as a distinctive fluorescent spot, starting at the free end of the molecule, which increased in brightness as more of the DNA was coiled into a toroid. The appearance of the fluorescent DNA molecules condensed by the proteins used in these experiments (Table I) were identical to those reported previously. Nevertheless it would be premature to assume that the DNA was, in fact, also condensed into toroids by TP1, TP2, and the synthesized peptides corresponding to their subdomains unless we verify this through further atomic force microscopy or electron microscopy of the condensed DNA molecules.

Determination of Protein Binding Rates—The rate of condensation of the DNA molecule has been previously shown to be linearly related to the concentration of the protein available for binding (31). Because the process of DNA condensation appears

[1] M. L. Meistrich (1998) personal communication.
[2] The abbreviations used are: HPLC, high performance liquid chromatography; DTT, dithiothreitol.
[3] D. Stigter, personal communication.

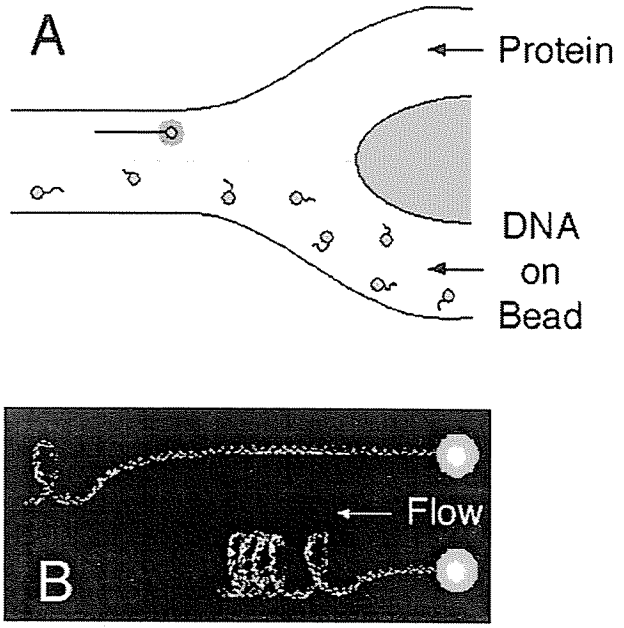

FIG. 1. *A*, dual-port flow cell. Individual DNA molecules attached to beads and protein flow side by side in a laminar fashion with little mixing. A single DNA molecule is held by an optical trap (*orange*) via its attached bead, and the extended DNA molecule is transported into the protein to observe the molecule condense as the protein binds. *B*, model showing how the condensation of DNA into a toroid is thought to occur. This has been experimentally verified for protamine but not for TP1 or TP2.

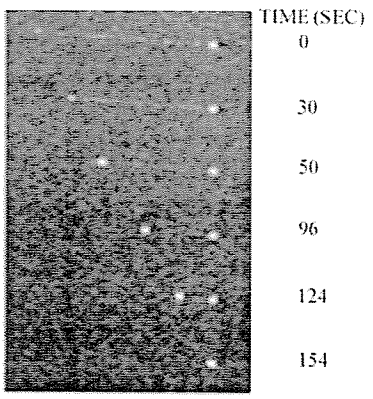

FIG. 2. **A series of time-lapse images of a 43-μm-long DNA molecule condensed by 3.0 μM SKRKAVRRRKRTHRAKRRTSGRRYK, a synthesized TP1 fragment.** The *bright, round object* on the *right* of the DNA image is an attached 1-μm-diameter bead held by the optical trap.

to be driven by the neutralization of the charge along the phosphodiester backbone as the basic nuclear protein or polycation binds (15, 16, 34, 35), the rate of protein binding to the DNA molecule can be determined by monitoring the rate of shortening of the DNA molecule. For each protein, a range of concentrations (~0–4 μM) was tested to determine whether the protein bound to the DNA molecule and condensed it. The condensation rate for 25–30 molecules was plotted as a function of protein concentration (Fig. 3). The data were fit to a straight line using a least-squares analysis, and the fitted slope was proportional to the binding rate constant, k_b. Dividing by the DNA binding footprint (if known) of the protein gave the binding rate constant. Footprints are known for hamster Protamine 1(10–11 bp) and Protamine 2 (15 bp) (36) but not TP1 or

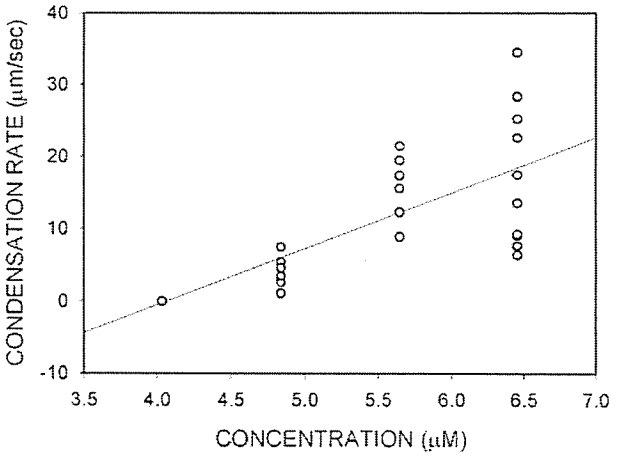

FIG. 3. **The condensation rate *versus* peptide concentration for SKRKAVRRRKRTHRAKRRTSGRRYK.** The slope of the least-squares fitted line is proportional to the binding rate for the peptide and is used to calculate, along with the protein dissociation rate, the dissociation constant, K_d.

TP2. Control experiments were also conducted using bovine serum albumin (3 μM), a protein that does not bind to DNA. In these experiments the DNA molecule remained fully extended throughout the duration of the experiment, which lasted several minutes. At this same concentration, DNA condensation times for all other proteins reported in this paper were typically much less than 1 min.

Experiments performed with hamster protamine 1 and protamine 2 showed that both protamines condense individual DNA molecules *in vitro*. These experiments, which were performed over a range of protein concentration (Table II), reveal that the two protamines appear to work equally well in condensing DNA. Protamine 2 condensation experiments, conducted with and without 50 μM zinc chloride, showed that the presence of the zinc increased the rate of protamine 2 binding to DNA nearly 3-fold.

Similar experiments conducted with hamster TP1 and TP2 showed that both transition proteins are capable of inducing DNA condensation. Both transition proteins condensed DNA at a rate similar to protamines 1 and 2. In contrast to the results obtained for protamine 2, the presence of 50 μM zinc chloride had no effect on the ability of TP2 to condense DNA.

Determination of Protein Dissociation Rates—The dissociation rates of the protamines and transition proteins were determined by pulling a DNA molecule into a low to moderate concentration of the protein (so it would not condense too rapidly), allowing it to condense to approximately one-half its length (to avoid nonspecific binding of the DNA-protein complexes to the streptavidin-coated bead), and then pulling the incompletely condensed DNA molecule back across the buffer interface, out of the protein solution and into the buffer stream containing only DNA. Using this approach, the upper limit of the dissociation rate of protein from the DNA molecule could then be determined by measuring the rate of re-extension of the DNA molecule (31). The mean and standard deviation of the dissociation rate constant, k_d, for ~10 DNA molecules is tabulated for each peptide in Table III. The dissociation constant, K_d, was determined by dividing the protein dissociation rate constant, k_d, by the binding rate constant, k_b, or if the protein footprint was not known, the decondensation rate divided by the condensation rate. The dissociation constant standard deviation was determined by using the standard propagation of uncorrelated errors.

Off-rates determined for both hamster protamine 1 and prot-

TABLE II

Rates of condensation of individual DNA molecules induced by spermatid basic nuclear proteins

k_b is the binding rate constant.

Protein	Condensation rate	k_b	Concentration range	Zinc	DTT
	$\mu m/s \cdot \mu M$	$s^{-1} \cdot \mu M^{-1}$	μM	50 μM	30 mM
Protamine 1	7.3 ± 0.9	1700 ± 210	0.0 – 4.0	No	Yes
Protamine 2	3.7 ± 1.4	620 ± 240	0.0 – 2.3	No	Yes
Protamine 2	10.6 ± 2.1	1800 ± 350	0.0 – 2.3	Yes	No
TP1	4.6 ± 0.5		0.0 – 3.1	No	Yes
TP2	4.9 ± 0.7		0.0 – 1.5	No	Yes
TP2	6.9 ± 1.2		0.0 – 1.2	Yes	No
SKRK...	7.7 ± 1.5		0.0 – 6.5	No	Yes
KRKY...	$1.4 \pm 0.44 \times 10^{-1}$		38.0 – 205.0	No	Yes
RRGKNR	No condensation		0.0 – 725.0	No	Yes

TABLE III

Rate of individual DNA molecule decondensation and protein off-rates for spermatid basic nuclear proteins

k_d is the dissociation rate constant, and K_d is the dissociation constant.

Protein	Decondensation rate	k_d	K_d	Zinc	DTT
	$\mu m/s$	s^{-1}	nM	50 μM	30 mM
TP1	$2.3 \pm 2.4 \times 10^{-2}$		5.0 ± 5.3	No	Yes
TP2	$4.0 \pm 2.8 \times 10^{-3}$		0.82 ± 0.58	No	Yes
TP2	$3.0 \pm 1.1 \times 10^{-3}$		0.44 ± 0.18	Yes	No
P2	$2.0 \pm 1.1 \times 10^{-3}$	0.34 ± 0.19	0.54 ± 0.36	No	Yes
P2	$2.0 \pm 0.64 \times 10^{-3}$	0.34 ± 0.11	0.19 ± 0.07	Yes	No
P1	$1.8 \pm 1.0 \times 10^{-3}$	0.41 ± 0.23	0.25 ± 0.14	No	Yes
P1	$1.5 \pm 0.65 \times 10^{-3}$	0.34 ± 0.15		Yes	No
SKRK...	$6.5 \pm 2.5 \times 10^{-3}$		0.84 ± 0.36	No	Yes
KRKY...	4.2 ± 3.1		$3.0 \pm 2.4 \times 10^{4}$	No	Yes

amine 2 were observed to be similar (~0.4–0.5 molecules/s) to those previously determined for salmine (0.7 molecules/s). Zinc had no effect on the rate of dissociation of either protamine. The transition protein TP1, by comparison, dissociated from DNA much more rapidly than either protamine. TP1 was measured to have a decondensation rate (the footprint is unknown) that was 10 times that of protamine 1. In contrast, the dissociation rate of TP2 from DNA was determined to be comparable to that of protamine 1 and protamine 2. As observed for protamine 2, zinc concentrations as high as 50 μM had no effect on the dissociation rate of TP2.

Binding and Dissociation of TP1 and TP2 Peptide Sequences—Condensation and off-rate experiments were also conducted with synthetic peptides, a 25-residue peptide corresponding to the carboxyl-terminal end of TP2 (SKRKAVRRRKRTHRAKRRTSGRRYK) and two arginine- and lysine-rich peptides present in TP1 (KRKYRKSVLKSRKR and RRGKNR). The rate of condensation and stability of the TP2-DNA complex and the TP2(25-mer)-DNA complex, as evidenced by their off-rates, were essentially identical. This was not observed for the TP1 peptides. Only one of the peptides (KRKYRKSVLKSRKR) was observed to condense DNA, and the rate of dissociation of this peptide from DNA was observed to occur at a much higher rate than observed for the TP1 (Table III).

DISCUSSION

DNA Condensation Induced by Protamines P1 and P2—In the present study, we have examined and compared the DNA binding kinetics of the four basic nuclear proteins (transition proteins TP1 and TP2 and protamines P1 and P2) that lead to the repackaging of chromatin during the final stages of mammalian spermatogenesis. These experiments not only show that both protamine 1 and 2 condense DNA, but they also demonstrate that protamine 2 is just as effective in condensing DNA as protamine 1. The rates of condensation achieved with hamster protamines in this study were similar to those observed previously (31) for equivalent concentrations of salmine.

Binding experiments conducted in the presence of zinc show that zinc increases the rate of protamine 2 binding to DNA nearly 3-fold, whereas it did not alter the rate of dissociation of protamine 2 from the DNA-protamine 2 complex. The effect of zinc on the protamine 2 on-rate is consistent with previous studies that have shown zinc binds to protamine 2 *in vitro* and with the hypothesis that zinc binding to protamine 2 may induce a structural change in the protein, such as the formation of a zinc finger that facilitates its binding to DNA (37, 38). Although a zinc-induced conformational change in protamine 2 has not been demonstrated, zinc is bound to protamine 2 *in vivo* in sperm chromatin (39), and its presence appears to be important for sperm chromatin function. Several studies have correlated zinc deficiencies in the male with infertility (40, 41).

Rate of Protamine Dissociation from DNA—Our analyses of the off-rates of the two hamster protamines have provided valuable new information that may be relevant to our understanding of how these proteins interact with DNA and perform their function. The off-rates determined for both hamster protamines were similar to the rate measured previously for salmine using the same technique (31). Although hamster protamines 1 and 2 contain cysteine residues that might form inter-protamine disulfide bonds and slow down the dissociation process (salmine does not contain cysteine), the current experiments were conducted in the presence of sufficient reducing agent (30 mM DTT) to preclude disulfide bond formation. These experiments also show that the off-rate determined for hamster protamine 2 is not significantly different from that observed for protamine 1. This indicates that the previously reported finding that sperm containing substantial amounts of protamine 2 decondenses more rapidly in the oocyte after fertilization (42) must not be caused by differences in the affinities of the two protamines for DNA.

The absence of an effect of zinc on the off-rate of protamine 2 also suggests that once protamine 2 is bound to DNA, its affinity is not dictated by the presence of the zinc or its ability to maintain a zinc finger (or some other) conformation. Those factors that stabilize the interaction between protamine 2 and DNA once it is bound, such as the bonds formed between the

arginine residues and the DNA backbone phosphates, may not differ significantly in protamine 2-DNA complexes formed with and without zinc.

TP1 and TP2 Condense DNA—Baskaran and Rao (20) have previously reported that TP2 condenses DNA *in vitro*. In these earlier studies, results were obtained that suggested that transition protein-induced condensation must be quite different from that achieved with protamine. TP1 was also reported to be less effective in condensing DNA than TP2 (20). The results we obtained using single DNA molecules show that both transition proteins TP1 and TP2 can condense free DNA *in vitro*, but comparisons of the decondensation rates of the TP1-DNA and TP2-DNA complexes obtained from these studies demonstrate that TP2 binds more tightly to DNA. The dissociation constant determined for TP2 (0.82 nM) was found to be similar to that of hamster protamines P1 (0.25 nM) and P2 (0.54 nM). TP1 was observed to bind DNA 6-fold less tightly (K_d = 5.0 nM). The TP1 and TP2 dissociation constants, which were obtained under conditions that prevented DNA aggregation and precipitation, are orders of magnitude lower than those measured by Baskaran and Rao (20).

The results obtained in the decondensation studies also suggest that the dissociation rate of hamster TP2, protamine 1 and protamine 2 are determined primarily by the sequences (and number of positively charged amino acids) of their DNA binding domains. As the earlier studies showed (31, 32) the off-rates for salmine (which contains 21 arginine residues/molecule) and Arg_6 (0.71 and 18,000 molecules/s, respectively) appear to be related to the number of arginine residues present in the molecule. The more arginine residues that are available to bind to the phosphodiester backbone of DNA, the lower the off-rate. Similar results were obtained in this study for both hamster protamines and TP2. Because TP2 binds to DNA with the same affinity as protamine, its seems likely that this protein may displace the histones directly by competing for DNA binding and initiating condensation. TP1, on the other hand, exhibits significantly weaker binding, which suggests that it may be less likely to displace histones simply by direct competition.

Role of Transition Protein Subdomains—Because both transition proteins condense DNA, these results suggest the arginine- and lysine-rich sequences in TP1 and TP2 participate in DNA binding in such a manner that they effectively neutralize the charge along the DNA backbone. TP2 appears to have two separate domains that contribute to its interaction with DNA. The amino-terminal three-quarters of the molecule has been reported to provide the specificity in the protein's binding to CpG sequences (21, 43), possibly through the formation of two or more zinc finger domains (44), while the carboxyl-terminal domain may play a major role in facilitating condensation (45). This hypothesis was confirmed for TP2 by condensation experiments conducted using only the carboxyl-terminal 25-mer of TP2: SKRKAVRRRKRTHRAKRRTSGRRYK. Experiments performed with this peptide revealed that both the rate of DNA condensation and rate of dissociation of the carboxyl-terminal TP2 peptide from DNA were indistinguishable from rates observed for the intact TP2 protein. This observation adds additional support to Kundu and Rao's hypothesis (21) that this sequence must be the DNA binding domain of TP2. It also shows that this sequence alone is sufficient to confer the DNA condensation properties of the protein. This result and our observation that the presence of zinc does not alter either the rate of DNA condensation induced by TP2 or the decondensation of the complex suggest that the remainder of the protein (the amino-terminal domain) may provide some sequence specificity in binding to CpG islands, but it cannot contribute significantly to the proteins binding affinity.

The rat and mouse TP1 sequences contain only three short positively charged segments with 4–5 arginine and lysine residues. Two peptides containing these sequences, RRGKNR and KRKYRKSVLKSRKR, were synthesized, and their ability to condense DNA was tested. In contrast to the results obtained with the TP2 peptide, neither TP1 peptide was effective in condensing DNA. The smaller peptide, RRGKNR, did not condense DNA. The larger peptide, KRKYRKSVLKSRKR, condensed DNA but only at extremely high concentrations. Working at a concentration 100-fold higher than that used for TP1, the rate of condensation induced by the peptide was observed to be only 1/30 of that observed with the intact TP1 protein. Similarly, the off-rate of the bound peptide was dramatically different, almost 200-fold faster than the off-rate measured for TP1. These differences in binding and complex stability demonstrate that the binding of TP1 to DNA must involve more than just the affinity contributed by the binding of either of the two arginine- and lysine-rich TP1 peptide sequences that were tested. Because only one of the two peptides bound and condensed DNA, it is highly unlikely that the simultaneous binding of both peptides could be responsible for the observed binding properties of TP1. Some other aspects of the three-dimensional structure of the TP1 protein must play an important role in its binding to DNA.

Relevance of Transition Protein Condensation of Free DNA—Although these experiments clearly show that the transition proteins can condense histone-free DNA, the relevance of this observation is not entirely certain. It is clear from electron microscopy studies that the deposition of the transition proteins on DNA in early spermatids is correlated with a noticeable change in the condensation state of chromatin (6), but the chromatin does not appear to achieve a level of compaction comparable with that attained when the protamines replace TP1 and TP2. Although TP1 and TP2 can bind to and condense free DNA, these proteins may not be able to induce the condensation of DNA when they bind to chromatin. The presence of the histones and the nucleosomal organization present in early spermatids could easily alter how the transition proteins interact with and condense the DNA.

Single Molecule Versus Ensemble Condensation Studies—These results clearly demonstrate the utility of single molecule binding studies to assess the kinetics of DNA condensation and determine protein dissociation rates. Previous studies of the binding of the protamines and transition proteins have been complicated by the aggregation and precipitation that occurs when these proteins bind to bulk DNA in solution. Using a single-molecule approach, the condensation process can be identified (torus formation *versus* nucleosome or other form of compaction) and the kinetics of the process (rates of protein binding and dissociation) can be measured directly. The results obtained in this study not only confirm the previous observation that the binding of TP1 and TP2 to DNA are different (20), but they have also provided new information showing that both proteins are capable of condensing histone-free DNA. Whether this actually is likely to occur in the spermatid, where the DNA is complexed with histone, remains to be determined.

Although these experiments provide new information about the kinetics of DNA condensation by the protamines and transition proteins, it is critical that future studies of this kind be conducted under conditions that will allow the sequential complexation of DNA with a series of proteins, to assess how effective individual proteins are in displacing histones and reorganizing the structure of chromatin under conditions more closely resembling that encountered *in vivo*. This should be possible in the near future, once we complete the construction of a multiport flow cell (which will enable the DNA molecule to

be moved through multiple protein solutions) and the preparation of defined lengths of DNA complexed with histones or chromatin fibers attached to beads.

REFERENCES

1. Meistrich, M. L. (1989) in *Histones and Other Basic Nuclear Proteins* (Hnilica, L. S., Stein, G. S., and Stein, J. L., eds) pp. 165–182, CRC Press, Orlando, FL
2. Kierszenbaum, A. L., and Tres, L. L. (1975) *J. Cell Biol.* **65,** 258–270
3. Balhorn, R., Weston, S., Thomas, C., and Wyrobek, A. J. (1984) *Exp. Cell Res.* **150,** 298–308
4. Balhorn, R., Cosman, M., Thornton, K., Krishnan, V. V., Corzett, M., Bench, G., Kramer, C., Lee, J., IV, Hud, N. V., Allen, M., Prieto, M., Meyer-Ilse, W., Brown, J. T., Kirz, J., Zhang, X., Bradbury, E. M., Maki, G., Braun, R. E., and Breed, W. (1999) in *The Male Gamete: From Basic Knowledge to Clinical Applications* (Gagnon, C., ed) pp. 55–70, Cache River Press, Vienna, IL
5. Alfonso, P. J., and Kistler, W. S. (1993) *Biol. Reprod.* **48,** 522–529
6. Oko, R. J., Jando, V., Wagner, C. L., Kistler, W. S., and Hermo, L. S. (1996) *Biol. Reprod.* **54,** 1141–1157
7. Kistler, W. S., Henriksen, K., Mali, P., and Parvinen, M. (1996) *Exp. Cell Res.* **225,** 374–381
8. Kundu, T. K., and Rao, M. R. (1996) *Biochemistry* **35,** 15626–15632
9. Caron, N., Veilleux, S., and Boissonneault, G. (2001) *Mol. Reprod. Dev.* **58,** 437–443
10. Kierszenbaum, A. L. (2001) *Mol. Reprod. Dev.* **58,** 357–358
11. Pogany, G. C., Corzett, M., Weston, S., and Balhorn, R. (1981) *Exp. Cell Res.* **136,** 127–136
12. Hud, N. V., Milanovich, F. P., and Balhorn, R. (1994) *Biochemistry* **33,** 7528–7535
13. Allen, M. J., Bradbury, E. M., and Balhorn, R. (1997) *Nucleic Acids Res.* **25,** 2221–2226
14. Ward, W. S., and Zalensky, A. O. (1996) *Crit. Rev. Eukaryot. Gene Expr.* **6,** 139–147
15. Hud, N. V., Downing, K. H., and Balhorn, R. (1995) *Proc. Natl. Acad. Sci. U. S. A.* **92,** 3581–3585
16. Bloomfield, V. A. (1997) *Biopolymers* **44,** 269–282
17. Vijayanathan, V., Thomas, T., Shirahata, A., and Thomas, T. J. (2001) *Biochemistry* **40,** 13644–13651
18. Caceres, C., Gimenez-Bonafe, P., Ribes, E., Wouters-Tyrou, D., Martinage, A., Kouach, M., Sautiere, P., Muller, S., Palau, J., Subirana, J. A., Cornudella, L., and Chiva, M. (1999) *J. Biol. Chem.* **274,** 649–656
19. Singh, J., and Rao, M. R. (1987) *J. Biol. Chem.* **262,** 734–740
20. Baskaran, R., and Rao, M. R. (1990) *J. Biol. Chem.* **265,** 21039–21047
21. Kundu, T. K., and Rao, M. R. (1995) *Biochemistry* **34,** 5143–5150
22. Meetei, A. R., Ullas, K. S., Vasupradha, V., and Rao, M. R. (2002) *Biochemistry* **41,** 185–195
23. Levesque, D., Veilleux, S., Caron, N., and Boissonneault, G. (1998) *Biochem. Biophys. Res. Commun.* **252,** 602–609
24. Corzett, M., Kramer, C., Blacher, R., Mazrimas, J., and Balhorn, R. (1999) *Mol. Reprod. Dev.* **54,** 273–282
25. Balhorn, R., Gledhill, B. L., and Wyrobek, A. J. (1977) *Biochemistry* **16,** 4074–4080
26. Kistler, W. S., Noyes, C., Hsu, R., and Heinrikson, R. L. (1975) *J. Biol. Chem.* **250,** 1847–1853
27. Kleene, K. C., Borzorgzadeh, A., Flynn, J. F., Yelick, P. C., and Hecht, N. B. (1988) *Biochim Biophys Acta* **950,** 215–220
28. Heidaran, M. A., Kozak, C. A., and Kistler, W. S. (1989) *Gene* **75,** 39–46
29. Kleene, K. C., Gerstel, J., and Shih, D. (1990) *Gene* **95,** 301–302
30. Yelick, P. C., Kozak, C., Kwon, Y. K., Seldin, M. F., and Hecht, N. B. (1991) *Genomics* **11,** 687–694
31. Brewer, L. R., Corzett, M., and Balhorn, R. (1999) *Science* **286,** 120–123
32. Balhorn, R., Brewer, L., and Corzett, M. (2000) *Mol. Reprod. Dev.* **56,** 230–234
33. Hud, N. V., Allen, M. J., Downing, K. H., Lee, J., and Balhorn, R. (1993) *Biochem. Biophys. Res. Commun.* **193,** 1347–1354
34. Manning, G. S. (1980) *Biopolymers* **19,** 37–59
35. Matulis, D., Rouzina, I., and Bloomfield, V. A. (2000) *J. Mol. Biol.* **296,** 1053–1063
36. Bench, G. S., Friz, A. M., Corzett, M. H., Morse, D. H., and Balhorn, R. (1996) *Cytometry* **23,** 263–271
37. Bianchi, F., Rousseaux-Prevost, R., Bailly, C., and Rousseaux, J. (1994) *Biochem. Biophys. Res. Commun.* **201,** 1197–1204
38. Gatewood, J. M., Schroth, G. P., Schmid, C. W., and Bradbury, E. M. (1990) *J. Biol. Chem.* **265,** 20667–20672
39. Bench, G., Corzett, M. H., Kramer, C. E., Grant, P. G., and Balhorn, R. (2000) *Mol. Reprod. Dev.* **56,** 512–519
40. Abbasi, A. A., Prasad, A. S., Rabbani, P., and DuMouchelle, E. (1980) *J. Lab. Clin. Med.* **96,** 544–550
41. Dincer, S. L., and Oz, S. G. (1990) *Hosp. Pract. (Off. Ed.)* **25,** 20
42. Perreault, S. D., Barbee, R. R., Elstein, K. H., Zucker, R. M., and Keefer, C. L. (1988) *Biol. Reprod.* **39,** 157–167
43. Sato, H., Akama, K., Kojima, S., Miura, K., Sekine, A., and Nakano, M. (1999) *Protein Expr. Purif.* **16,** 454–462
44. Meetei, A. R., Ullas, K. S., and Rao, M. R. (2000) *J. Biol. Chem.* **275,** 38500–38507
45. Cole, K. D., and Kistler, W. S. (1987) *Biochem. Biophys. Res. Commun.* **147,** 437–442

THE JOURNAL OF BIOLOGICAL CHEMISTRY Vol. 278, No. 43, Issue of October 24, pp. 42403–42408, 2003
Printed in U.S.A.

Dynamics of Protamine 1 Binding to Single DNA Molecules*

Received for publication, April 7, 2003, and in revised form, August 8, 2003
Published, JBC Papers in Press, August 11, 2003, DOI 10.1074/jbc.M303610200

Laurence Brewer‡§, Michele Corzett¶, Edmond Y. Lau¶, and Rod Balhorn¶‖

From the ‡Electronic Engineering Technologies Division and ¶Biology and Biotechnology Research Program, Lawrence Livermore National Laboratory, Livermore, California 94550

Protamine molecules bind to and condense DNA in the sperm of most vertebrates, packaging the sperm genome in an inactive state until it can be reactivated following fertilization. By using methods that enable the analysis of protamine binding to individual DNA molecules, we have monitored the kinetics of DNA condensation and decondensation by protamine 1 (P1) and synthetic peptides corresponding to specific segments of the bull P1 DNA binding domain. Our results show that the number of clustered arginine residues present in the DNA binding domain is the most important factor affecting the condensation and stability of the DNA-protamine complex prior to the formation of inter-protamine disulfide cross-links. The high affinity of P1 for DNA is achieved by the coordinated binding of three anchoring domains, which together in bull P1 contain 19 Arg residues. The single DNA molecule experiments show that sequences containing two or more anchoring domains have an off-rate that is at least 3 orders of magnitude slower than those containing a single domain. The use of Arg, rather than Lys residues, and the inclusion of Tyr or Phe residues in the hinge regions between anchoring domains provide additional stability to the complex.

Several different mechanisms have been identified for packaging DNA in eucaryotic cells. The best understood is the packaging scheme used to organize DNA inside the nucleus of all somatic cells, in which the histones coil the DNA into 11-nm nucleosomal subunits that are further organized into 30-nm chromatin fibers. This type of packaging allows individual genes to be activated or repressed depending on the needs of the cell. In contrast, small basic nuclear proteins called protamines bind to the entire length of the haploid genome in sperm cells and coil 50-kb segments of DNA into ~60-nm toroidal subunits (1–4). Protamine binding maintains the DNA in this highly compact and transcriptionally inactive state for extended periods of time (5–8) until the sperm fertilizes an oocyte and its genome is reactivated.

Although a variety of protamine-like proteins have been isolated from different vertebrate sperm, only two distinct types of protamines, protamine 1 (P1) and protamine 2 (P2), package DNA in mammalian sperm. P1 has been found to be present in the sperm of every species examined (9, 10) and is the most abundant protein present in the sperm of many mammals (10, 11). Both P1 and P2 package DNA in rodent and primate sperm.

Sequence analyses of numerous P1 molecules and their genes have revealed that all mammalian P1 molecules appear to have several sequence-related features in common. The Arg residues that comprise the DNA binding domain of P1 are usually clustered in the center of the molecule (1, 10) in a series of DNA "anchoring domains." These anchoring domains, which typically contain 3–7 Arg residues (1), are usually separated by one or more uncharged amino acids. The interspersed amino acids linking the anchoring domains appear to function as a hinge, enabling the anchoring domains to wrap around the major groove of the DNA helix (12–14) and optimize the interactions that form between each Arg residue in the DNA binding domain of P1 and the negatively charged phosphates in the phosphodiester backbone of the two DNA strands (14). One P1 molecule appears to be bound to each turn of DNA (15, 16) such that the charge associated with each phosphate group in both strands of DNA is neutralized by an Arg residue of the bound P1. Ser and Thr residues located in the amino- and carboxyl-terminal peptide segments flanking the DNA binding domain have been shown to be phosphorylation sites that are believed to be modified prior to the deposition of P1 on DNA so that it binds correctly (17–19).

The protamines of eutherian mammals also contain numerous cys residues that are used to form intra- (20) and inter-protamine disulfide cross-links (10) during the final stages of sperm chromatin maturation. Intramolecular disulfide cross-links begin forming in late-step spermatids, shortly after the protamines bind to DNA. As the spermatids leave the testis and begin moving through the epididymis, a final set of disulfide bonds is formed that covalently link each protamine to its neighbor. This creates a chromatin complex that is highly compact and transcriptionally inert.

Previous studies using salmon protamine (salmine) (21), bull and boar P1 (8, 22), chicken protamine (23), and various oligoarginine or oligolysine peptides (24–28) have shown that the large number of basic amino acids present in the DNA binding domain of protamine enables it to condense DNA. Although the exact structure of the complex has not yet been determined, Raman spectroscopy and other studies have suggested that P1 must bind to DNA in an extended conformation with a footprint that covers ~11 bp of sequence (14, 16, 29).

In an effort to gain additional insight into how the protamines interact with DNA and inactivate the genes of the developing spermatid, we have examined the functions of specific subsets of the P1 DNA binding domain that enable protamine to bind to DNA and condense it into toroids. These experiments extend previous studies that have been conducted by others using various Arg- and Lys-containing oligopeptides (24–28) and focus on elucidating how three specific features of the P1 sequence affect the ability of P1 to bind to DNA and maintain it in a condensed state as follows: 1) the number of poly(Arg)

* This work was supported in part by the United States Department of Energy by the University of California, Lawrence Livermore National Laboratory, under Contract W-7405-Eng-48. The costs of publication of this article were defrayed in part by the payment of page charges. This article must therefore be hereby marked "*advertisement*" in accordance with 18 U.S.C. Section 1734 solely to indicate this fact.

§ Supported by NICHD Grant 1 K25 HD01387-03 from the National Institutes of Health.

‖ To whom correspondence should be addressed. Tel.: 925-422-6284; Fax: 925-422-2282; E-mail: balhorn2@llnl.gov.

clusters or anchoring domains, 2) the relative importance of Arg and Lys residues in these domains, and 3) the presence of aromatic amino acids interspersed between anchoring domains. Peptides corresponding to subdomains of the bull P1 sequence were synthesized, and kinetics of their binding to individual λ phage DNA molecules were examined under conditions that preclude intermolecular aggregation (21).

EXPERIMENTAL PROCEDURES

Peptide Synthesis and Purification—Bull P1 was isolated from pooled bull semen (American Breeders Service, DeForest, WI) and purified using high performance liquid chromatography as described previously (11). The peptide sequences synthesized for this study used bull P1 as the primary reference sequence, ARYRCCLTHSGSRCRRRRRRCRRRRRRFGRRRRRRVCCRRYTVIRCTRQ. The bull P1 sequence shares a strong consensus with the sequences for P1 molecules found in other mammals (10).

Peptides corresponding to various subsets of the bull P1 sequence were synthesized by SynPep Corp. (Dublin, CA) and were purified by high performance liquid chromatography. Electrospray mass spectrometry was used to confirm their sequence and purity. Peptides located in the DNA binding domain of P1 were synthesized with an acetylated amino terminus and an amide on the carboxyl terminus to minimize terminal charge effects and mimic the internal peptide sequences present in P1. The amino-terminal protamine peptide ARYRSSLTHSGSRS was synthesized with a carboxyl-terminal amide group, and the carboxyl-terminal protamine peptide VSSRRYTVIRSTRQ was synthesized with an amino-terminal acetyl group.

Protein Concentration Verification—To obtain accurate concentrations of the nuclear proteins used in the condensation experiments, the purified peptides and bull P1 were dissolved in 0.1% trifluoroacetic acid, known aliquots were distributed into glass tubes, and the samples were frozen and lyophilized. Replicate samples were dissolved in 6 N hydrochloric acid and hydrolyzed at 105 °C for 16 h, and the amino acid content of each tube was determined by AAA Service Laboratory (Boring, OR). The protein content of each sample was determined using the known sequence of bull P1 and the synthetic peptides. Tube to tube variations in the aliquoted samples used for the experimental studies were found to be less than 2%.

Preparation of Stained DNA Bead Sample—λ phage DNA (Sigma) was dissolved in buffer (degassed 50% sucrose (w/v), 100 mM sodium bicarbonate, pH 8, 30 mM dithiothreitol), tagged with biotin, and attached to 1-μm streptavidin-coated polystyrene spheres as described previously (21). YOYO-1 dye was then added so that the dye molecule to DNA base pair ratio was 1:4. Experiments performed with salmine and various peptides have shown that this concentration of YOYO-1 does not alter the kinetics of binding to DNA (21). The same buffer, minus the YOYO-1 dye, was used to dissolve the protein samples. In experiments involving the binding and dissociation of bull P1 to DNA, dithiothreitol was included to prevent the formation of disulfide bonds between P1 molecules following their binding to DNA.

Condensation / Decondensation Experiments—The experimental apparatus is identical to that used previously to examine the condensation of individual DNA molecules by salmon protamine (21). Separate solutions containing protein and DNA molecules attached to polystyrene beads were introduced into a dual port flow cell at a flow velocity of ~50 μm/s where they flowed side by side, in a laminar fashion, with little mixing. Beads containing individual DNA molecules were trapped using an infrared laser optical trap (λ = 1.047 μm). An argon ion laser (λ = 488 nm) was used to excite the YOYO-1-stained DNA molecules, and their fluorescence was visualized using an image-intensified CCD camera.

Working at a depth of about 20 μm below the coverslip (the flow cell depth was 40 μm), the DNA molecule was pulled across the interface separating the two flowing buffer solutions, and the shortening of individual DNA molecules was monitored as the protein or peptide bound to it and induced condensation. The condensed DNA was evident as a bright fluorescent spot at the end of the DNA molecule. The length of the stained λ phage DNA molecule (48.5 kb) extended by flow was measured to be 19.2 ± 0.82 μm at a flow rate of 72 μm/s in 50% sucrose. Under these conditions, the DNA was 95% extended.[1]

Analyses of Protein and Peptide Binding Kinetics—The condensation rates for 5–20 individual DNA molecules were measured at several different protein or peptide concentrations, and a linear least squares fit (in conjunction with the peptide footprint) was used to determine the binding, or "on-rate", k_{on}, of the peptide or protein to DNA. The binding of peptides and proteins to DNA was shown previously to be the rate-limiting step in condensation, and the length of the DNA molecule during condensation was shown to decrease linearly with time (21, 30) (Fig. 1, *A* and *B*). The decondensation rate was determined by pulling partially condensed DNA molecules back to the DNA side of the flow cell (where there was an absence of peptide or protein) and observing the DNA re-extend as the bound peptide left the DNA. The mean of ~10 molecules was used to determine the "off-rate," k_{off}, of each peptide or protein dissociating from the DNA molecule. The dissociation constant K_d was determined by dividing the off-rate by the on-rate, $K_d = k_{off}/k_{on}$.

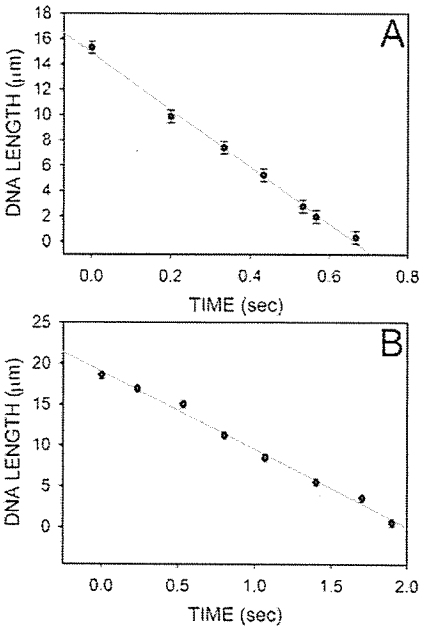

FIG. 1. **A single DNA molecule is pulled from the DNA side of a two-channel flow cell into buffer containing peptide or protein, and the length of the molecule is recorded (*blue dots*) as a function of time as it condenses.** This is shown for 100 μM Arg_6 (*A*) and 2.4 μM bull P1 (*B*). A least square fit of the data (*green line*) indicates that the DNA molecule condenses linearly with time for both Arg_6 and bull P1. A kinetic analysis of the data suggests that protein or peptide binding occurs only from the free end of the DNA molecule in flow.

Computational Analysis of Peptide Solution Conformation Using Molecular Dynamics—Molecular dynamics simulations were performed with AMBER (31) using the Cornell force field (32). Structures of the R_6GGR_6 and R_6FGR_6 peptides were constructed in extended conformations and solvated in boxes of TIP3P water (33) sufficient in size to have at least 15 Å of water between the protein and the solvent interface (81 × 72 × 45 $Å^3$ initially). Twelve chloride ions were added to each system to neutralize the charge. The systems typically consisted of 21,400 atoms (~7,000 water molecules). Each system was energy-minimized using 250 steps of steepest descents and 750 steps of conjugate gradients. Constant temperature and pressure dynamics were performed on these energy-minimized systems. Periodic boundary conditions were used, and electrostatic interactions were treated by Particle Mesh Ewald methods (34) with a 9-Å cut-off in direct space, cubic interpolation, and using a 1-Å grid. SHAKE (35) was used to constrain bonds containing a hydrogen, and a time step of 2 fs was used. These systems were coupled to a heat bath at 300 K. Coupling constants of 5 and 2 ps were used for peptide and solvent, respectively. Each simulation was performed for a total of 2.5 ns, and the last 2.0 ns were used for analysis. Coordinates were saved every 200 time steps. The peptide conformers were clustered using the program NMRCORE (36). Solvent-accessible surface areas were calculated using the program surfv (37).

RESULTS

Rate of DNA Condensation by P1 and Peptides—The rates of DNA condensation induced by the binding of bull P1 and a series of peptides containing different sequences present in the bull P1 DNA binding domain (Arg^{15}–Arg^{36}; sequence ARYRC-

[1] D. Stigter, personal communication.

TABLE I
Rate of condensation of individual DNA molecules induced by bull P1 and synthesized proteins

Protein	Condensation rate	On-rate (k_{on})	Concentration range
	$\mu m/s \cdot \mu M$	*molecules/s·μM*	*μM*
Bull P1	9.2 ± 1.8	2113 ± 413	0–2.6
Arg_6	$2.1 \pm 0.4 \times 10^{-1}$	177 ± 34	0–200
Lys_6	$2.7 \pm 0.25 \times 10^{-2}$	23 ± 2	0–1800
R_6YGR_6	$3.3 \pm 0.7 \times 10^{-1}$	139 ± 30	0–73
R_6FGR_6	$8.3 \pm 1.5 \times 10^{-1}$	350 ± 63	0–19
R_6GGR_6	8.8 ± 0.96	3711 ± 405	0–5
K_6GGK_6	$7.6 \pm 1.0 \times 10^{-1}$	320 ± 42	0–44
RKRKRKGGRKRKRK	$6.5 \pm 0.7 \times 10^{-1}$	274 ± 30	0–82
$R_6GGR_6GGR_6$	3.3 ± 0.7	926 ± 197	0–11
Acetyl-VSSRRYTVIRSTRQ	No condensation		2.1
$ARYRSSLTHSGSRS\text{-}CONH_2$	No condensation		2.4

CLTHSGSRCRRRRRRRCRRRRRRFGRRRRRRVCCRRYTVIRCTRQ) were determined for a range of protein and peptide concentrations (Table I). The results show that the rate of DNA condensation is affected by the number of Arg residues in the peptide or the protein's DNA binding domain, the presence of an aromatic residue in the hinge region between anchoring domains, and the substitution of Lys for Arg residues. Arg_6 was the least effective of the Arg-containing peptides in condensing DNA. While R_6GGR_6 condensed the DNA molecules 42 times faster than Arg_6, increasing the number of Arg_6 anchoring domains from two to three, as in bull P1 and $R_6GGR_6GGR_6$, did not increase the rate of condensation. Bull P1 and R_6GGR_6 condensed DNA with equal rates, while the condensation rate for $R_6GGR_6GGR_6$ was surprisingly smaller. Substituting an aromatic residue for one of the Gly residues in R_6GGR_6 resulted in condensation rates that were a factor of 10–25 smaller (R_6YGR_6 and R_6FGR_6). The substitution of Lys residues for Arg also altered the rate of condensation. Lys_6 was observed to be 10-fold less effective in condensing DNA than Arg_6, and K_6GGK_6 was nearly 10-fold less effective than R_6GGR_6. Substitutions of individual Arg residues with Lys also decreased the condensation rate (Table I).

Peptides corresponding to the amino-terminal ($ARYRSSLTHSGSRS\text{-}CONH_2$) and carboxyl-terminal ($CH_3CO\text{-}VSSRRYTVIRSTRQ$) sequences of P1 outside the DNA binding domain were tested for their ability to condense DNA at concentrations similar to those used for the peptides containing anchoring domain sequences. The Ser residues were substituted for Cys to eliminate the possibility that the peptides might form disulfide-linked folded forms (38) or multimers in solution and complicate our interpretation of the results. No DNA condensation was observed for either peptide at a concentration of 2 μM. While these results suggest that the amino- and carboxyl-terminal sequences flanking the protamine DNA binding domain do not bind to DNA, we cannot exclude the possibility that the cysteine residues normally present in these sequences may stabilize the formation of some disulfide-dependent conformation in the peptide that enables DNA binding.

Protein and Peptide Off-rates Determined by Decondensation—The DNA decondensation rates and dissociation constants (K_d) measured for bull P1, and the synthetic peptides are shown in Table II. Bull P1 remained attached to DNA for the longest period of time with a dissociation rate (k_{off} = 0.23 molecules/s) that was similar to previous rates obtained for salmine and hamster P1 (8, 21, 30) The peptide sequences $R_6GGR_6GGR_6$, R_6GGR_6, and RKRKRKGGRKRKRK dissociated from DNA at faster rates (k_{off} = 6–7 molecules/s), while Arg_6 and Lys_6 dissociated from DNA much more rapidly (k_{off} = 17,000 and 9,000 molecules/s, respectively). K_6GGK_6 dissociated from DNA at a significantly faster rate (k_{off} = 25 molecules/s) than R_6GGR_6.

The inclusion of an aromatic amino acid between two Arg_6 domains also appeared to increase the stability of the peptide-DNA complex. Sequences containing Tyr had substantially slower off rates than those containing only Gly. The inclusion of a single Tyr residue decreased the off-rate of the peptide by 6-fold. Peptides containing Phe exhibited a similar, but less pronounced effect. Replacing the first Gly in R_6GGR_6 with Phe decreased the off-rate by 2-fold.

Computational Simulation of the Protamine Anchoring Domain by Using Molecular Dynamics—Molecular dynamics runs were performed on the R_6GGR_6 and R_6FGR_6 peptides to examine how the presence of the aromatic Phe residue located between two anchoring domains might affect the conformation adopted by the adjacent peptide segments and ultimately impact the binding of these sequences to DNA. Structures of each peptide were constructed in extended conformation and solvated in boxes of water utilizing periodic boundaries. Molecular dynamics simulations were run for a total time of 2.5 ns using a fixed number of particles held at constant pressure and temperature.

Clustering analysis performed on 200 structures selected at 10-ps intervals during the last 2.0 ns of the simulations are shown in Fig. 2, *A* and *B*. Comparisons of these structures suggest that both peptides form a significant amount of structure along the backbone of the entire sequence. In the simulation performed with the R_6GGR_6 sequence, this backbone remains reasonably extended as a result of the extension and solvation of the Arg side chains. The mobility of the carboxyl-terminal region of this peptide is constrained by the formation of a salt bridge between the terminal carboxyl group and the side chain of residue Arg^{11}. The most interesting structure, however, is that developed in the R_6FGR_6 peptide during the last 1.1 ns of the simulation. In this peptide, the phenyl ring stacks against the peptide backbone and appears to form a stable core that is surprisingly tight (Fig. 2*B*). In these structures, the aromatic ring of Phe interacts with the backbone amides of Gly^8 and Arg^9. One consequence of this stacking is that the backbone is bent between the two anchoring (Arg_6) domains.

The distances measured from the amide hydrogen to the center of mass of the Phe ring during the last nanosecond of the simulation are 3.88 ± 0.63 and 3.52 ± 0.42 Å for Gly^8 and Arg^9, respectively. One effect of the interaction between the aromatic ring and backbone is that the amount of motion sampled by the ring is reduced significantly. The positional fluctuation of the Phe side chain is 4.54 Å for the first nanosecond of dynamics but reduces to 2.72 Å when stacked against the peptide backbone. The average solvent-accessible surface area of R_6FGR_6 (2766.5 ± 87.4 Å^2) is lower than for R_6GGR_6 (2850.4 ± 79.4 Å^2) even though R_6FGR_6 has the greater intrinsic surface area.

TABLE II
Decondensation rate of individual DNA molecules and associated dissociation constants (K_d) for bull P1 and synthesized proteins

Protein	Decondensation rate	Off-rate (k_{off})	K_d
	μm/s	*molecules/s*	*M*
Bull P1	$1.0 \pm 0.6 \times 10^{-3}$	0.23 ± 0.14	$1.1 \pm 0.7 \times 10^{-10}$
Arg_6	20.1 ± 5.0	16800 ± 4200	$9.6 \pm 3.0 \times 10^{-5}$
Lys_6	11.0 ± 3.4	9260 ± 2860	$4.1 \pm 1.3 \times 10^{-4}$
R_6YGR_6	$2.6 \pm 0.8 \times 10^{-3}$	1.1 ± 0.33	$7.9 \pm 2.9 \times 10^{-9}$
R_6FGR_6	$7.9 \pm 3.3 \times 10^{-3}$	3.3 ± 1.4	$9.5 \pm 4.3 \times 10^{-9}$
R_6GGR_6	$1.6 \pm 0.7 \times 10^{-2}$	6.7 ± 3.0	$1.8 \pm 0.8 \times 10^{-9}$
K_6GGK_6	$5.9 \pm 2.8 \times 10^{-2}$	24.8 ± 11.8	$7.8 \pm 3.8 \times 10^{-8}$
RKRKRKGGRKRKRK	$1.7 \pm 0.6 \times 10^{-2}$	7.2 ± 2.5	$2.6 \pm 1.0 \times 10^{-8}$
$R_6GGR_6GGR_6$	$2.2 \pm 0.4 \times 10^{-2}$	6.2 ± 1.1	$6.7 \pm 1.9 \times 10^{-9}$

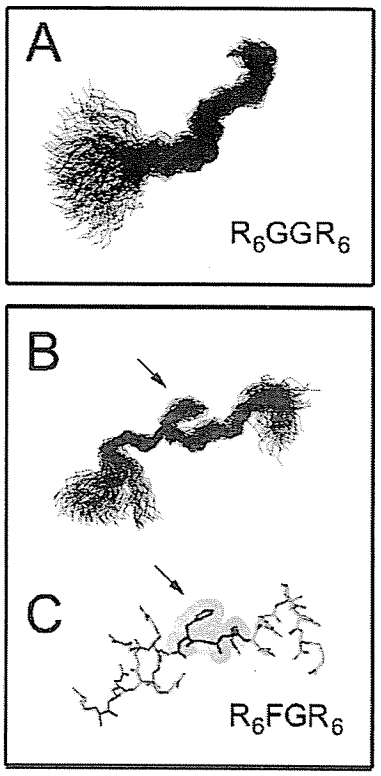

FIG. 2. *A*, the superposition of the backbone atoms of R_6GGR_6 from molecular dynamics calculations. Only the N, CA, and C atoms of the peptide are shown. A total of 200 structures, taken from 10-ps intervals, are shown. *B*, overlay of the backbone atoms for R_6FGR_6 from the last 1.16 ns of molecular dynamics calculations (116 structures). Only the N, CA, and C atoms of the peptide are shown for clarity. *C*, the last of the 116 structures shown in *B*. The Phe and backbone atoms of Gly^8 and Arg^9 are drawn as Corey-Pauling-Koltun space-filling models (49). The *arrows* in *B* and *C* point to the aromatic ring of Phe^7 that stacks against the backbone amides of Gly^8 and Arg^9.

DISCUSSION

Importance of Multiple Arg_6 DNA Anchoring Domains—DNA condensation and decondensation experiments were performed using a series of synthetic peptides containing one (Arg_6), two (R_6GGR_6), and three ($R_6GG\ R_6GGR_6$) Arg_6 anchoring sequences as model subsets of the bull P1 DNA binding domain and two 14-residue peptides corresponding to the amino-terminal and carboxyl-terminal sequences flanking the bull P1 DNA binding domain. Even though the sequences of the model peptides do not correspond to the exact sequences present in bull P1 (the Cys residues were changed to Ser or Gly to prevent disulfide bond formation and model anchoring domains containing six Arg residues separated by two Gly residues were used to build up a peptide sequence corresponding to a "representative" P1 DNA binding domain), these experiments clearly showed that each of the peptides containing one or more Arg_6 anchoring sequences bound to and condensed DNA. In contrast, neither the synthetic amino-terminal nor carboxyl-terminal P1 peptide sequences condensed DNA.

The number of Arg residues present in the anchoring domain peptides had a significant effect on both the concentration of the peptide required to condense DNA and the stability of the complexes. While even a single Arg_6 anchoring domain condensed DNA, condensation could only be achieved at peptide concentrations that were 44-fold higher than those used for bull P1. Rates of Arg_6 binding to DNA were observed to be 12-fold lower than the rate of bull P1 binding at equivalent concentrations. The ineffectiveness of Arg_6 in condensing DNA was also seen in the instability of the Arg_6-DNA complex. By increasing the number of Arg_6 anchoring domains present in the peptide sequence from one to two (R_6GGR_6), the rate of dissociation of the peptide from the complex was reduced by 2500-fold.

Surprisingly, increasing the number of anchoring domains in the synthetic peptides from two to three did not increase either the effectiveness of the peptide in condensing DNA or the stability of the complex. R_6GGR_6 bound to and condensed DNA at rates similar to those observed for bull P1, but this rate was 2.7 times faster than that achieved with $R_6GGR_6GGR_6$. In addition, the stability of the R_6GGR_6 and $R_6GGR_6GGR_6$-DNA complexes, as reflected by the rates of dissociation of the peptides, was identical. These results show that the rate of binding, and the stability of the resulting complex, are not strictly determined by the number of Arg residues in the P1 DNA binding domain but suggest that other factors must be involved. One factor that may contribute to the rate of binding is the increase in flexibility inherent in longer peptides. Once the length of the binding domain increases beyond two anchoring domains, the increased flexibility of the sequence could adversely influence the rate of binding and condensation.

Formation and Relative Stability of Complexes Formed with Lys-containing Anchoring Domains—Previous studies (26, 39) have shown that the Arg residues in peptides and proteins bind more tightly to DNA than Lys residues because the guanidinium group in Arg forms both a hydrogen bond and salt bridge to the phosphate groups that comprise the backbone of DNA. Several different groups have examined and compared the ability of peptides containing sequences with multiple Lys or Arg residues to bind and condense DNA (26–28, 39, 40). The majority of this work focused on small (dimer to tetramer) or high molecular weight Arg or Lys polymers.

One study found that increasing the number of Lys residues in short (2–3-mers) homopolymers increases the affinity of the peptide for double-stranded DNA (24). A second study found that larger homopolymers of Arg are more effective in inducing DNA aggregation and precipitation (27). Binding affinities have not been determined or compared in previous studies for peptides above tetramers. Experiments conducted with KXK

and KXXK peptides containing aromatic amino acids also provided evidence that aromatic amino acids located between two Lys residues did exhibit a detectable but small effect on the base sequence preference for peptides binding to DNA (24, 39, 41). These previous studies also provided evidence that the insertion of non-basic amino acids between Lys or Arg residues in short homopolymers eliminated the base sequence specificity that has been observed for poly(Lys) and poly(Arg) binding to duplex DNA (24).

In the present study, experiments conducted with one or two Lys_6 anchoring domains showed that they were remarkably ineffective in condensing DNA compared with Arg-containing peptides. At least a 10-fold higher concentration of the Lys-containing peptides was required to achieve a condensation rate similar to that of Arg-containing peptides. Once bound, however, Lys was as effective as Arg in maintaining DNA in a condensed state. To within experimental error, peptides of the same length, composed of Lys and/or Arg residues, containing GG in the hinge region between domains, and corresponding to one (Arg_6 and Lys_6) or two (R_6GGR_6, K_6GGK_6, and RKRKRKGGRKRKRK) anchoring domains, had the same off-rate. The DNA condensation and binding rate of K_6GGK_6 and RKRKRKGGRKRKRK were essentially identical. This suggests that the dominant factor contributing to DNA binding in sequences containing at least two anchoring domains is the number of positively charged side chains available for binding to the phosphodiester backbone of DNA.

Contribution of Aromatic Amino Acids to DNA Binding and Complex Stability—Mammalian and other vertebrate protamines frequently contain Tyr or Phe residues located within the DNA binding domain (11, 23, 42). Bull P1, used as the model P1 sequence for these experiments, contains a single Phe residue positioned between two Arg_6 anchoring domains. Decondensation experiments conducted with the bull P1 sequence R_6FGR_6, and its analogs, R_6GGR_6 and R_6YGR_6, showed that the presence of an aromatic amino acid increased the stability of the DNA-peptide complex by decreasing the off-rate of the peptides. R_6YGR_6 formed the most stable complex (k_{off} = 1.1 molecules/s), followed by R_6FGR_6 (k_{off} = 3.3 molecules/s) and R_6GGR_6 (k_{off} = 6.7 molecules/s), respectively. These results and the difference in off-rates observed for bull P1 and $R_6GGR_6GGR_6$ indicate that these aromatic amino acids probably do contribute to the overall stability of the DNA-protamine complex.

As has been observed for other DNA-binding proteins (1, 43–46), the aromatic ring of Tyr or Phe may intercalate between base pairs or bind in the groove through hydrophobic interactions or hydrogen bonding. Numerous sites are available inside the major groove for hydrogen bonding to the Tyr hydroxyl group, including the amino groups of cytosine and adenine, the N-7 groups of guanine and adenine, and the carbonyl oxygen of thymine or guanine. Although the current experiments do not provide enough information to enable us to discriminate between these possibilities, preliminary NMR studies of a complex formed between a hairpin DNA and a slightly different but related P1 sequence containing Phe have indicated that the phenyl ring is intercalated (1). The insertion of this ring between base pairs would force the DNA molecule to bend. Bends in the DNA-protamine complex would be expected to facilitate, and may even initiate, toroid formation.

The 10–30-fold slower on-rate we observed for R_6XGR_6 sequences containing an aromatic amino acid and the molecular dynamics simulations of the conformation adopted by the peptides in solution are both consistent with binding that involves an intercalation event. The results of the molecular dynamics simulation of the conformation of the R_6FGR_6 peptide suggest that the aromatic side chain may stack against the backbone of two adjacent amino acids (Gly^8 and Arg^9), lowering the hydration state of the peptide and kinking the backbone slightly. Aromatic ring-backbone interactions are not uncommon and have been shown to occur in other proteins (47, 48). In contrast, the equivalent peptide containing only Gly residues in the hinge region (R_6GGR_6) remains extended throughout the simulation. These results suggest that anchoring domain sequences separated by an aromatic amino acid should take longer to bind to DNA in a manner that optimizes the interactions of the Arg residues in the anchoring domains with the phosphodiester backbone of the DNA. Once the first anchoring domain binds to DNA, additional time would be required for the aromatic side chain to unstack with the protein backbone and insert into the helix before the second anchoring domain could bind properly to the phosphodiester backbone of DNA.

The stacking of the aromatic ring of Phe or Tyr against the peptide backbone might also be expected to reduce, somewhat, the flexibility of larger sequences, such as bull P1, that contain a third anchoring domain. This could explain the differences we observed for the on-rates of bull P1 and the model DNA binding domain $R_6GGR_6GGR_6$. Whereas the presence of an aromatic amino acid between two Arg_6 anchoring domains reduced the rates of peptide binding and DNA condensation (R_6GGR_6 *versus* R_6FGR_6 and R_6YGR_6) 10–30-fold, its presence is a sequence containing three anchoring domains (bull P1) increased the rate of peptide binding to DNA (P1 *versus* $R_6GGR_6GGR_6$) by 2–3-fold.

Information About the Site of Protein/Peptide Binding Derived from Kinetics—Analyses of the binding kinetics of salmine obtained in a previous study (21) and bull P1 and Arg_6 in this study (Fig. 1, *A* and *B*) have revealed that the length of an individual DNA molecule undergoing condensation decreases linearly with time. In each study we have observed that the binding of these proteins or peptides is the rate-limiting step in the condensation process. It follows that the rate of binding of these molecules to DNA is constant and time-independent. The first order equation describing the protein on-rate is given by Equation 1,

$$d/dt[BS] = k_{on} \cdot [P][FS] \quad \text{(Eq. 1)}$$

where $[FS]$ is the concentration of free binding sites on the DNA molecule; $[P]$ is the protein concentration; $[BS]$ is the concentration of bound sites on the DNA, and k_{on} is the on-rate for protein binding to DNA. The rate of increase of the bound sites on the DNA molecule, $d/dt[BS]$, is equal in magnitude and opposite in sign to rate of the decrease in length of the DNA molecule. Clearly, the only way that this term can be time-independent is if $[P]$ and $[FS]$ are also time-independent. Because the binding experiments are performed in a flow stream that provides a constant concentration of protein, $[P]$ remains constant throughout the course of the experiment. If $[FS]$ is constant, this means that the number of binding sites available for peptide/protein binding during the condensation process is fixed. If all remaining binding sites were equally available, the binding of protein would vary exponentially with time.

One interpretation of these results is that the fixed binding site (or sites) is located at the point where the DNA bends and is condensed into the toroid, which starts in our experimental system at the free end of the extended DNA molecule. If this interpretation of the data is correct, the constant rate of condensation suggests that the protein/peptide can only bind to the DNA if the DNA is bent to a dimension on the order of its persistence length (toroids are 50 nm (3)). Whereas this hypothesis is intriguing, the best way to verify this theory is by

designing experiments that enable the direct visualization of the site of protein binding.

Relationship between DNA Binding Domain Sequence and Protamine Function—The results obtained from these single molecule DNA condensation studies have provided new insight into the features of the sequence of the P1 DNA binding domain that facilitate its function. As these experiments have demonstrated, relatively low concentrations of the protein are required to condense DNA and maintain it in a condensed state for extended periods of time if the DNA binding domain contains multiple Arg_6 anchoring domains. This is particularly important in mammals because the maturation process for the developing sperm can take as long as 2–3 weeks, and the disulfide bonds that cross-link the DNA-bound protamines together (so they cannot dissociate or be displaced from DNA) are not formed until very late in the sperm maturation process (during epididymal transit).

These extremely low off-rates also suggest that large concentrations of unbound protein are not required to maintain the entire genome in an inactive, condensed state. The low off-rate of the protamine molecule is particularly important in those non-mammalian vertebrates that use protamines to package their sperm DNA. Because the protamines in these species do not contain Cys, inter-protamine disulfide bonding cannot be used to stabilize the final structure of the mature sperm chromatin complex.

The results of these studies also appear to provide a plausible "rationale" for why protamines tend to be arginine-rich rather than lysine-rich DNA-binding proteins. Because DNA is condensed most effectively by protamines with DNA binding domains that are composed almost exclusively of Arg, selective pressures applied by the sperm during the evolution of the sequence of the protamine DNA binding domain should select against the use of Lys residues as replacements for Arg. This appears to be generally the case. Occasional Lys residues can be found in the DNA binding domains of several mammalian protamines, but they are never clustered together as the only components of an entire anchoring domain in P1.

Acknowledgments—We thank Cheryl Dolan and Monique Cosman for proofreading the manuscript.

REFERENCES

1. Balhorn, R., Cosman, M., Thornton, K., Krishnan, V. V., Corzett, M., Bench, G., Kramer, C., Lee, J., IV, Hud, N. V., Allen, M., Prieto, M., Meyer-Ilse, W., Brown, J. T., Kirz, J., Zhang, X., Bradbury, E. M., Maki, G., Braun, R. E., and Breed, W. (1999) in *The Male Gamete: From Basic Knowledge to Clinical Applications* (Gagnon, C., ed) pp. 55–70, Cache River Press, Vienna, IL
2. Allen, M. J., Bradbury, E. M., and Balhorn, R. (1997) *Nucleic Acids Res.* **25,** 2221–2226
3. Hud, N. V., Allen, M. J., Downing, K. H., Lee, J., and Balhorn, R. (1993) *Biochem. Biophys. Res. Commun.* **193,** 1347–1354
4. Ward, W. S., and Zalensky, A. O. (1996) *Crit. Rev. Eukaryotic Gene Expr.* **6,** 139–147
5. Meistrich, M. L. (1989) in *Histones and Other Basic Nuclear Proteins* (Hnilica, L. S., Stein, G. S., and Stein, J. L., eds) pp. 165–182, CRC Press, Inc., Boca Raton, FL
6. Hecht, N. B. (1998) *BioEssays* **20,** 555–561
7. Sassone-Corsi, P. (2002) *Science* **296,** 2176–2178
8. Balhorn, R., Brewer, L., and Corzett, M. (2000) *Mol. Reprod. Dev.* **56,** 230–234
9. Corzett, M., Mazrimas, J., and Balhorn, R. (2002) *Mol. Reprod. Dev.* **61,** 519–527
10. Balhorn, R. (1989) in *Molecular Biology of Chromosome Function* (Adolph, K. W., ed) pp. 366–395, Springer-Verlag Inc., New York
11. Mazrimas, J. A., Corzett, M., Campos, C., and Balhorn, R. (1986) *Biochim. Biophys. Acta* **872,** 11–15
12. Prieto, M. C., Maki, A. H., and Balhorn, R. (1997) *Biochemistry* **36,** 11944–11951
13. Feughelman, M., Langridge, R., Seeds, W. E., Stokes, A. R., Wilson, H. R., Hooper, C. W., Wilkins, M. H. F., Barclay, R. K., and Hamilton, L. D. (1955) *Nature* **175,** 834–838
14. Hud, N. V., Milanovich, F. P., and Balhorn, R. (1994) *Biochemistry* **33,** 7528–7535
15. Pogany, G. C., Corzett, M., Weston, S., and Balhorn, R. (1981) *Exp. Cell Res.* **136,** 127–136
16. Bench, G. S., Friz, A. M., Corzett, M. H., Morse, D. H., and Balhorn, R. (1996) *Cytometry* **23,** 263–271
17. Louie, A. J., and Dixon, G. H. (1972) *J. Biol. Chem.* **247,** 7962–7968
18. Chirat, F., Arkhis, A., Martinage, A., Jaquinod, M., Chevaillier, P., and Sautiere, P. (1993) *Biochim. Biophys. Acta* **1203,** 109–114
19. Pirhonen, A., Linnala-Kankkunen, A., and Menpaa, P. H. (1994) *Eur. J. Biochem.* **223,** 165–169
20. Balhorn, R., Corzett, M., Mazrimas, J., and Watkins, B. (1991) *Biochemistry* **30,** 175–181
21. Brewer, L. R., Corzett, M., and Balhorn, R. (1999) *Science* **286,** 120–123
22. Tobita, T., Tanimoto, T., and Nakano, M. (1988) *Biochem. Int.* **16,** 163–173
23. Nakano, M., Kasai, K., Yoshida, K., Tanimoto, T., Tamaki, Y., and Tobita, T. (1989) *J. Biochem. (Tokyo)* **105,** 133–137
24. Standke, K. C., and Brunnert, H. (1975) *Nucleic Acids Res.* **2,** 1839–1849
25. Wehling, K., Arfmann, H. A., Standke, K. H., and Wagner, K. G. (1975) *Nucleic Acids Res.* **2,** 799–807
26. Mascotti, D. P., and Lohman, T. M. (1997) *Biochemistry* **36,** 7272–7279
27. Kawashima, S., and Ando, T. (1978) *J. Biochem. (Tokyo)* **84,** 343–350
28. Olins, D. E., Olins, A. L., and Von Hippel, P. H. (1967) *J. Mol. Biol.* **24,** 157–176
29. Zhang, X., Balhorn, R., Mazrimas, J., and Kirz, J. (1996) *J. Struct. Biol.* **116,** 335–344
30. Brewer, L., Corzett, M., and Balhorn, R. (2002) *J. Biol. Chem.* **277,** 38895–38900
31. Pearlman, D. A., Case, D. A., Caldwell, J. W., Ross, W. S., Cheatham, T. E., III, Debolt, S., Ferguson, D., Seibel, G., and Kollman, P. A. (1995) *Comput. Phys. Commun.* **91,** 1–41
32. Cornell, W. D., Cieplak, P., Bayly, C. I., Gould, I. R., Merz, K. M., Ferguson, D. M., Spellmeyer, D. C., Fox, T., Caldwell, J. W., and Kollman, P. A. (1995) *J. Am. Chem. Soc.* **117,** 5179–5197
33. Jorgensen, W. L., Chandrasekhar, J., Madura, J. D., Impey, R. W., and Klein, M. L. (1983) *J. Chem. Phys.* **79,** 926–935
34. Essmann, U., Perera, L., Berkowitz, M. L., Darden, T., Lee, H., and Pedersen, L. G. (1995) *J. Chem. Phys.* **103,** 8577–8593
35. Ryckaert, J. P., Ciccotti, G., and Berendsen, H. J. C. (1977) *J. Comput. Phys.* **23,** 327–341
36. Kelley, L. A., Gardner, S. P., and Sutcliffe, M. J. (1997) *Protein Eng.* **10,** 737–741
37. Sridharan, S., Nicholls, A., and Honig, B. (1992) *FASEB J.* **6,** A174
38. Balhorn, R., Corzett, M., and Mazrimas, J. A. (1992) *Arch. Biochem. Biophys.* **296,** 384–393
39. Porschke, D. (1978) *Eur. J. Biochem.* **86,** 291–299
40. Kawashima, S., Inoue, S., and Ando, T. (1969) *Biochim. Biophys. Acta* **186,** 145–157
41. Brun, F., Toulme, J. J., and Helene, C. (1975) *Biochemistry* **14,** 558–563
42. Sautiere, P., Belaiche, D., Martinage, A., and Loir, M. (1984) *Eur. J. Biochem.* **144,** 121–125
43. Coleman, J. E., and Armitage, I. M. (1978) *Biochemistry* **17,** 5038–5045
44. Buck, F., Hahn, K. D., Zemann, W., Ruterjans, H., Sadler, J. R., Beyreuther, K., Kaptein, R., Scheek, R., and Hull, W. E. (1983) *Eur. J. Biochem.* **132,** 321–327
45. Huang, X., Shullenberger, D. F., and Long, E. C. (1994) *Biochem. Biophys. Res. Commun.* **198,** 712–719
46. Wong, B., Masse, J. E., Yen, Y. M., Giannikopoulos, P., Feigon, J., Johnson, R. C., and Giannikoupolous, P. (2002) *Biochemistry* **41,** 5404–5414
47. Worth, G. A., and Wade, R. C. (1995) *J. Phys. Chem.* **99,** 17473–17482
48. Toth, G., Watts, C. R., Murphy, R. F., and Lovas, S. (2001) *Proteins Struct. Funct. Genet.* **43,** 373–381
49. Corey, R. B., and Pauling, L. (1953) *Rev. Sci. Instrum.* **24,** 621–627

Packaging of Single DNA Molecules by the Yeast Mitochondrial Protein Abf2p

Laurence R. Brewer,* Raymond Friddle,†‡ Aleksandr Noy,† Enoch Baldwin,‡ Shelley S. Martin,‡ Michele Corzett,§ Rod Balhorn,§ and Ronald J. Baskin‡

*Electronics Engineering Technologies Division, †Chemistry and Materials Science Division, and §Biology and Biotechnology Division, Lawrence Livermore National Laboratory, Livermore, California 94550 USA; and ‡Department of Molecular and Cellular Biology and Graduate Group in Biophysics University of California at Davis, Davis, California 95616 USA

ABSTRACT Mitochondrial and nuclear DNA are packaged by proteins in a very different manner. Although protein-DNA complexes called "nucleoids" have been identified as the genetic units of mitochondrial inheritance in yeast and man, little is known about their physical structure. The yeast mitochondrial protein Abf2p was shown to be sufficient to compact linear dsDNA, without the benefit of supercoiling, using optical and atomic force microscopy single molecule techniques. The packaging of DNA by Abf2p was observed to be very weak as evidenced by a fast Abf2p off-rate ($k_{off} = 0.014 \pm 0.001\ s^{-1}$) and the extremely small forces (<0.6 pN) stabilizing the condensed protein-DNA complex. Atomic force microscopy images of individual complexes showed the 190-nm structures are loosely packaged relative to nuclear chromatin. This organization may leave mtDNA accessible for transcription and replication, while making it more vulnerable to damage.

INTRODUCTION

Mitochondrial (mt) DNA is packaged into discrete units known as "nucleoids" in both yeast and man, and these structures have been shown to be the genetic units of mitochondrial inheritance (Garrido et al., 2003; Jacobs et al., 2000; MacAlpine et al., 2000). However, little is known about nucleoid formation or composition (MacAlpine et al., 2000). The density with which mtDNA is packaged affects both its maintenance and its accessibility during regulatory processes such as replication and transcription. Indeed, mtDNA is thought to be more susceptible to free radical induced damage than nuclear DNA (O'Rourke et al., 2002; Richter et al., 1988) in part because of a lack of protective histone packaging, and this type of damage has been proposed to lead to late-onset neurodegenerative disorders (Menzies et al., 2002; O'Rourke et al., 2002).

Abf2p is a mitochondrial (mt) protein that has been hypothesized to play a major role in packaging mtDNA into nucleoids (Caron et al., 1979; MacAlpine et al., 2000; Megraw and Chae, 1993; Newman et al., 1996) in the yeast *Saccharomyces cerevisiae*. Abf2p also contributes to mtDNA maintenance (Contamine and Picard, 2000), copy number (Cho et al., 2001; Zelenaya-Troitskaya et al., 1998), transcription (Diffley and Stillman, 1991, 1992), and recombination (MacAlpine et al., 1998). It is closely related in sequence and function to the vertebrate nuclear high-mobility group (HMG) protein HMG1 (Diffley and Stillman, 1992) and is a homolog of human mitochondrial transcription factor h-mtTFA (Fisher et al., 1992; Parisi et al., 1993), a protein implicated in human mitochondrial disease (Wallace, 2002; Wredenberg et al., 2002). Recently, h-mtTFA was identified as the protein responsible for human mtDNA packaging (Alam et al., 2003). Both HMG1 and h-mtTFA bend DNA and introduce supercoils into circular DNA molecules.

We used two different experimental techniques to demonstrate and provide complementary information about the compaction of DNA by Abf2p. Optical trapping of single DNA molecules extended by flow and visualized by fluorescence microscopy has been used to obtain information about the kinetics of binding and force with which the Abf2p-DNA complex is packaged. Atomic force microscopy (AFM) confirmed that DNA is bent by Abf2p, and provided a high resolution view and the dimensions of the compact Abf2p-DNA complex.

MATERIALS AND METHODS

Purification of Abf2p

The *Saccharomyces cerevisiae* ABF2 gene in a pMalc2X fusion vector (Kao et al., 1993) (New England BioLabs, kindly provided by the Nunnari Lab, University of California Davis) was cloned into pET28b(+) (Novagen, Madison, WI). Inverse polymerase chain reaction was used to fuse an initiator methionine and six histidine codons to the ABF2 reading frame encoding mature Abf2p, residues 21 to 177 with his tag, M_r = 19,484 Daltons. Protein was purified from BL21(DE3)(pET28b-His_6ABF2) cultures (5–10 mg/L culture), essentially as described for Cre recombinase (Martin et al., 2002) except 500 mM NaCl was used in the initial lysis buffer, and the solution was dialyzed to low salt buffer before ion exchange chromatography. Concentrated and filtered samples, 20–70 mg/mL (Millipore Centricon-10) (Billerica, MA) in 20 mM Na-HEPES pH 7.5, 1 mM Na-EDTA, 4 mM DTT, 0.1 w/v Na-azide, were diluted with 10 mM Tris-Cl pH 7.8, 4 mM DTT, 1 mM Na-EDTA. Abf2p concentrations were determined using an extinction coefficient at 280 nm of 1.29 $mg^{-1}mL$, or 24,180 M^{-1}. DNA binding activity was established with a gel-retardation assay (Cho et al., 2001) using either supercoiled pLitmus-38(+) or linear lambda-phage DNA (New England BioLabs, Beverly, MA) as a substrate.

Optical trapping measurements

To obtain information about the binding kinetics of Abf2p to DNA, single, linear, lambda-phage DNA molecules attached to beads were held by an

Submitted April 24, 2003, and accepted for publication June 23, 2003.

Address reprint requests to L. Brewer, E-mail: brewer1@llnl.gov.

0006-3495/03/10/2519/06 $2.00

optical trap and extended by flowing buffer in a two-channel flow cell (Fig. 1, *a* and *b*) as previously described (Brewer et al., 1999). The buffer used in these experiments, 100 mM $NaHCO_3$ (pH 8), contained no sucrose.

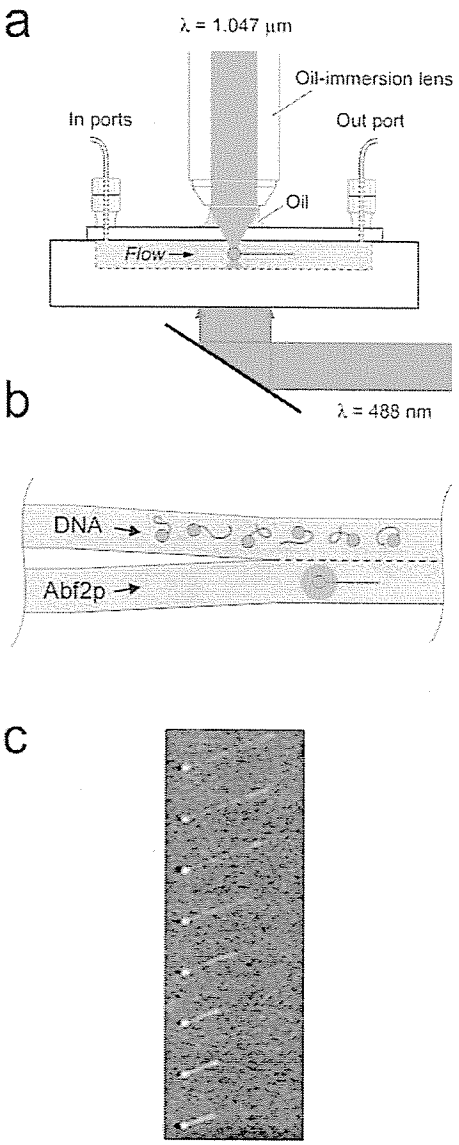

FIGURE 1 (*a*) Side view of the flow cell showing the trapping and excitation laser beams. (*b*) Top view of the flow cell. An individual DNA molecule held by an optical trap (*orange*) via its attached bead, and extended by flowing buffer, is moved into protein solution by translating the stage holding the flow cell perpendicular to the direction of flow. DNA was stained with YOYO-1 dye, allowing the compaction to be observed using fluorescence microscopy. The molecule was then moved back to the DNA side of the flow cell (which was protein-free), and the decompaction of the molecule was observed as protein left it, ultimately returning to its original length. (*c*) Time-lapse images of a lambda-phage DNA dimer (35 μm contour length) undergoing compaction by Abf2p. The Abf2p concentration is 2 μM. The time interval between successive frames is 0.5 s. The buffer flow speed is 63 μm/s.

Measurement of buffer flow velocity

Flow cell buffer velocities were determined by releasing the bead from the optical trap at the conclusion of each compaction/decompaction measurement and determining the distance the bead moved in a given time.

Measurement of maximal tether force

A value for the tether force (Stigter and Bustamante, 1998; Zimm, 1998) of the compacted DNA-Abf2p complex was determined by first reducing the trapping laser power so that the maximal force, sometimes called the escape force, the optical trap could exert on a 1-μm-diameter bead was 1.4 pN. A maximal value for the "tether force" (the force with which Abf2p-compacted DNA pulls on its attached bead due to hydrodynamic friction) was determined by subtracting the Stokes force on the bead attached to the compacted DNA molecule from the calibrated trap force, as long as the DNA molecule plus bead could be held by the trap while it compacted. The trap force was determined by moving the microscope stage holding a sample cell containing buffer and 1-μm-diameter beads at successively faster velocities until a trapped bead was released from the optical trap. The Stokes force, $6\pi\eta rv$, was then used to calculate the force on the bead at the point of release, where η is the buffer viscosity, r is the bead diameter, and v is the stage velocity. The bead was held at a position 10–15 μm beneath the surface of the coverslip, so that no corrections had to be made for the surface. The sample cell consisted of a microscope slide, a drop of buffer containing beads, and a coverslip supported by two 50 μm thick plastic shims. The four sides of the coverslip were attached to the slide by nail polish.

Data analysis

The rate equation describing the binding of Abf2p to DNA for a first order process can be written as follows:

$$d/dt[U] = k_{on}[U][\text{Abf2p}] - k_{off}[B], \tag{1}$$

where $[U]$, $[B]$, and [Abf2p] represent the concentration of unbound DNA sites, bound DNA sites, and Abf2p, respectively, and k_{on} and k_{off} are the rate constants for protein binding and releasing from a single DNA molecule. The length of the DNA molecule itself is proportional to the amount of protein bound to the DNA molecule since protein binding is the rate-limiting step (see Results and Discussion). In Eq. 1, [Abf2p] = 0 when the DNA molecule is on the DNA side of the flow cell. Also, as we shall see, k_{off} is much smaller than k_{on} so we can neglect the term $k_{off}[B]$ when describing binding. The sum of the unbound and bound sites on the DNA molecule is equal to the total number of binding sites:

$$N_o = U + B. \tag{2}$$

Using Eqs. 1 and 2 we can solve for the rates and find for the compaction process that

$$[U] = [N_o]\exp - k_{on}[\text{Abf2p}]t \tag{3}$$

and similarly for the decompaction process

$$[U] = [N_o](1 - \exp - k_{off}t). \tag{4}$$

The length versus time plots (Fig. 2) for the compaction and decompaction processes for an individual DNA molecule of length L were then fit to the following equations:

$$L(t) = (L - L_2)\exp - k_{on}[\text{Abf2p}]t + L_2 \tag{5}$$

$$L(t) = (L - L_2)(1 - \exp - k_{off}t) + L_2. \tag{6}$$

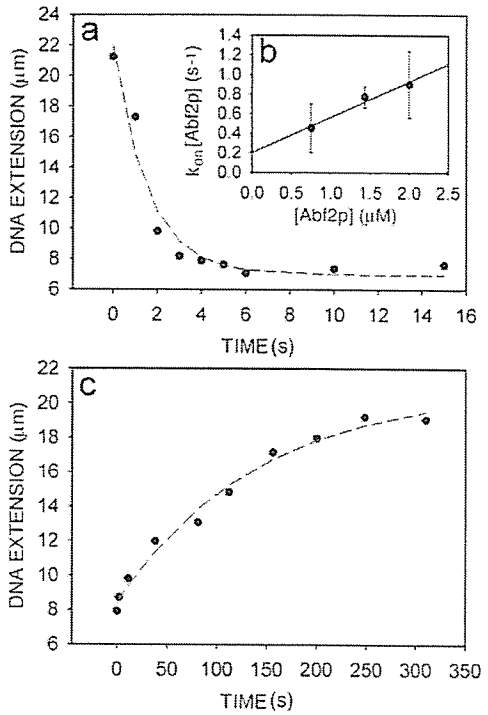

FIGURE 2 (*a*) Compaction of a single DNA molecule by Abf2p in 1.43 μM Abf2p ($k_{on} = 0.45 \pm 0.1\ \mu M^{-1}\ s^{-1}$). (*b*) Linear variation of Abf2p binding rate (k_{on}[Abf2p]) with Abf2p concentration ($k_{on} = 0.36 \pm 0.1\ \mu M^{-1}\ s^{-1}$). (*c*) Decompaction of the same DNA molecule as in *a* ($k_{off} = 7.0 \pm 1.3 \times 10^{-3}\ s^{-1}$). The data in *a* and *c* are given by black points, and the exponential fit is represented by a red line.

L_2 is the length of the compacted Abf2p-DNA complex, which can be directly measured; L is the initial length of the DNA molecule, which is measured, so the fit is really only a one-parameter fit to k_{off}, or k_{on}[Abf2p] where [Abf2p] is known.

Effect of YOYO-1 dye on Abf2p binding

The extension of 16 lambda-phage DNA molecules stained with YOYO-1 dye in buffer without protein were measured at different flow velocities. Extensions were calculated from different DNA contour lengths (Stigter and Bustamante, 1998) to compare with the measured values. The contour length which best fit the data was 17.6 μm (mean error in extension fit was 4%) using a persistence length of 55 nm. The contour length of unstained lambda-phage DNA is 16.4 μm, and values of the length of stained DNA have been reported as high as 22 μm (Brewer et al., 1999; Perkins et al., 1995). We infer that the amount of YOYO-1 dye bound to the DNA is much less than the saturating ratio of 1 YOYO-1 dye molecule per 4 bp and do not expect YOYO-1 to affect the binding of Abf2p protein to DNA.

AFM measurements

High resolution atomic force microscopy (AFM) was used to observe the interactions between Abf2p and linear dsDNA (pBR322 was linearized by digesting with BamH1. The DNA was then washed four times in a Centricon-100 concentrator in 10 mM Tris, 1 mM EDTA pH 8 to remove enzyme and twice in 100 mM $NaHCO_3$ to buffer exchange). The microscope, a Nanoscope IIIa (Digital Instruments, Woodbury, NY), was used in tapping mode with Si FESP probes (NanoWorld, Neuchâtel, Switzerland). Abf2p and DNA in buffer (100 mM $NaHCO_3$ pH 8) were mixed together for 5 min before depositing on a substrate. The substrate was prepared by applying 3 μL of 0.1% aqueous solution of poly-L-lysine (Sigma, St. Louis, MO) to a freshly cleaved mica surface for 1 min. The sample was then rinsed with distilled water and dried with nitrogen. The concentration of DNA in the mixed solution remained fixed at 1 μg/mL, and the Abf2p concentration varied from 1.5 μg/mL to 25 μg/mL. Data analysis was performed using IgorPro software (Lake Oswego, OR).

RESULTS AND DISCUSSION

Kinetics of Abf2p binding

The compaction and decompaction of single DNA molecules by Abf2p is shown in Fig. 1 *c* and Fig. 2. Notable features of the compaction and decompaction plots (Fig. 2, *a* and *c*) are their exponential shape, which is indicative of a first order kinetic process, and the finite length of the compacted DNA molecule. The percent compaction varied between 50% and 89% and increased as the length of the DNA molecule (Fig. 3) and flow velocity (data not shown) decreased.

The binding of Abf2p to DNA was shown to be the rate-limiting step in the compaction of DNA. By moving the translation stage holding the flow cell in the same direction as the flowing buffer we were able to increase the effective velocity of buffer containing Abf2p and observe the length of a partially compacted DNA molecule (100% compaction was never achieved; see Fig. 3) increase significantly. Upon stopping the stage, the protein-DNA complex rapidly returned to its initial length in ~1 s, which was much faster than the timescale observed for compaction. This result

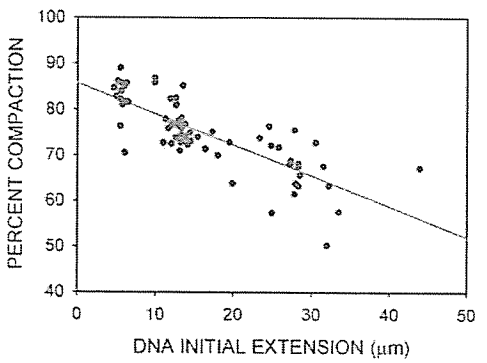

FIGURE 3 DNA compaction versus initial extension for 67 molecules in 2 μM Abf2p, taken at buffer flow speeds between 50 and 110 μm/s. The compaction is defined as the difference between the initial (no protein) and final (in protein) DNA extensions divided by the initial DNA extension. For the range of DNA contour lengths and buffer flow velocities used in our experiment, the fractional extension of the DNA was fairly constant: 76 ± 5% (Perkins et al., 1995; Stigter and Bustamante, 1998). The incomplete compaction is thought to be due to the extension of the Abf2p-DNA complex by the flowing buffer. The longer the initial DNA contour length, the greater the hydrodynamic drag of the compacted Abf2p-DNA complex, and the less compaction is observed. The linear least squares fit is represented by a green line.

shows that the rate-limiting step in the compaction of the Abf2p-DNA complex is the rate of Abf2p binding to DNA. From this experiment we also deduced that at least part of the incomplete compaction of the Abf2p-DNA complex was due to the elongation of the protein-DNA complex by the flowing buffer.

The data and fit (using Eq. 5 and Eq. 6) for the compaction and decompaction of a single DNA molecule by Abf2p are shown in Fig. 2, *a* and *c*. We measured the on-rate at three different Abf2p concentrations (Fig. 2 *b*) and the binding rate determined from the exponential fit, $k_{on}[b]$ varied linearly with concentration, as expected. The on-rate constant, $k_{on} = 0.36 \pm 0.1\ \mu M^{-1}\ s^{-1}$, did not depend on either the initial DNA extension (at constant flow speed) or flow velocity. Decompaction measurements (10 molecules) allowed us to determine $k_{off} = .014 \pm 0.001\ s^{-1}$. The ratio of these rates, k_{on}/k_{off}, provided the binding constant $K_b = 2.57 \pm 0.74 \times 10^7\ M^{-1}$.

Limit on binding from the McGhee-von Hippel theory

The maximal fractional coverage of DNA by Abf2p, which can be calculated from the equilibrium constant, K_b, Abf2p footprint (~27 bp (Diffley and Stillman, 1991, 1992), and Abf2p concentration (2 μM) using the McGhee-von Hippel theory (McGhee and von Hippel, 1974) equals 87%. The greatest observed compaction of DNA by Abf2p was 89% (Fig. 3). Measurements obtained from AFM images (Fig. 4) of individual compact Abf2p-DNA complexes showed a reduction in length of DNA from 1.5 μm to 190 nm, a compaction of 87%. These results indicate that 13% of each DNA molecule was not bound with Abf2p.

Abf2p compaction force

The most direct approach to determine the strength with which Abf2p packages DNA is to pull on both ends of the compacted DNA molecule and measure the force versus extension curve (Baumann et al., 2000; Wang et al., 1997). Another approach, which is suitable for measuring very small compaction forces, is to use flowing buffer to extend the compacted Abf2p-DNA complex (held by an optical trap) and measure its tether force (Stigter and Bustamante, 1998; Zimm, 1998). The tether force is the hydrodynamic drag the flowing buffer exerts on the protein-DNA complex, and it provides an estimate of the forces needed to elongate DNA bound by Abf2p. Fig. 3 shows how the percent compaction DNA by Abf2p decreases as the length of the DNA molecule increases. This is what one would expect if the tether, or drag, force of the Abf2p-DNA complex is sufficient to overcome the forces that maintain the complex in a compacted state. Using this approach, we have measured the maximal tether force for 15 different DNA molecules bound with Abf2p. Initial DNA extensions ranged from 5 to 15 μm, and compactions range from 72% to 89%. We find that the mean tether force $\leq 0.60 \pm 0.12$ pN. This suggests it takes very little force to elongate DNA compacted by Abf2p and the forces that stabilize the compacted protein-DNA complex are quite weak.

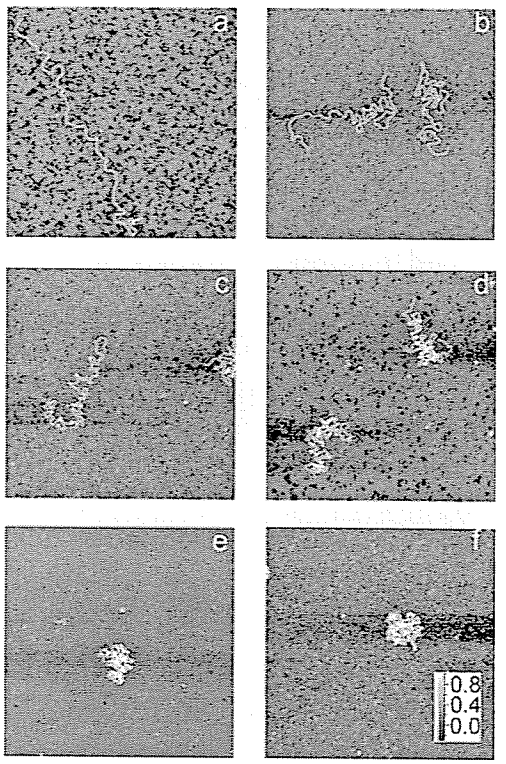

FIGURE 4 AFM images (image scale is 1 μm along each axis, height scale (*f*) is in nm) of Abf2p protein bound to single linear dsDNA molecules (pBR322, 1.5 μm contour length, 4361 bp). The DNA is bent and compacted as the concentration of Abf2p increases, ultimately forming a compact, 190 ± 90 nm diameter, round object. The ratio of Abf2p molecules to DNA bp is as follows with Abf2p concentrations indicated in parenthesis: (*a*) 0.0 Abf2p/bp (0 μM), (*b*) 0.04 Abf2p/bp (0.075 μM), (*c*) 0.1 Abf2p/bp (0.175 μM), (*d*) 0.2 Abf2p/bp (0.35 μM), (*e*) 0.45 Abf2p/bp (0.75 μM), and (*f*) 0.75 Abf2p/bp (1.25 μM). For an Abf2p footprint of 27 bp, the DNA coverage is complete for an Abf2p-to-bp ratio of 0.037.

AFM images

AFM images of Abf2p-DNA complexes (Fig. 4, *a–f*) show sharp bending of DNA by Abf2p. As the concentration of Abf2p increases, the DNA becomes increasingly compact, finally forming a round object with diameter 190 ± 90 nm. The ratio of Abf2p molecules to DNA bp (Abf2p/bp) for the complexes imaged in Fig. 4 *b* is 0.04, allowing Abf2p to fill all available binding sites on the DNA molecule for a 27-bp footprint. However, complete DNA compaction was not observed until the Abf2p/bp ratio reached 0.45. This is consistent with our calculations of the equilibrium fractional

coverage of DNA by Abf2p, given by k_{on}[Abf2p]/k_{off}, where [Abf2p] denotes the concentration of Abf2p, $k_{on} = 0.36 \pm 0.1\ \mu M^{-1}\ s^{-1}$, and $k_{off} = 0.014 \pm 0.001\ s^{-1}$. For [Abf2p] = 0.04 μM (Fig. 4 *b*), the fractional coverage equals 50% and some bending is seen, whereas when [Abf2p] = 0.35 μM (Fig. 4 *d*), the fraction coverage equals 90%, and almost complete compaction of the individual DNA molecules is observed. However, the McGhee-von Hippel theory limits the fractional coverage to 85% for [Abf2p] = 1 μM, and this may explain why the degree of compaction in images Fig. 4, *e* and *f* look similar.

We have shown that Abf2p obeys first order binding kinetics to linear DNA. The measured on-rate constant, ($k_{on} = 0.36 \pm 0.1\ \mu M^{-1}\ s^{-1}$), together with an estimated concentration of Abf2p in the mitochondria, can be used to determine the compaction time for the mitochondrial genome. For a mitochondria with ellipsoidal dimensions of 0.5 μm (radius) by 1.0 μm, and 50 genome equivalents of mtDNA (MacAlpine et al., 2000), the concentration of Abf2p is 540 μM (assuming complete coverage of the DNA by Abf2p). This concentration multiplied by the measured on-rate constant gives an exponential time constant of 194 s^{-1}. Clearly, mtDNA will be rapidly packaged by Abf2p. The off-rate of Abf2p from DNA was measured to be $k_{off} = 0.014 \pm 0.001\ s^{-1}$. This implies that in the absence of free Abf2p, the time needed for all the bound protein to dissociate from mtDNA would be several minutes. Therefore, Abf2p is not strongly bound to DNA compared to the histones (Brower-Toland et al., 2002) that organize nuclear DNA or protamine (Brewer et al., 1999), which packages DNA in the sperm cell. This implies that a significant concentration of free Abf2p must be maintained in the mitochondria to keep the mtDNA in a compact state, which is consistent with the calculation above of the Abf2p concentration in the mitochondria.

The tether force measured for DNA molecules compacted by Abf2p was extremely small, $\leq 0.60 \pm 0.12$ pN, showing that the forces holding the Abf2p-DNA complex together are weak. AFM measurements of the spatial extent of single DNA molecules bound with Abf2p showed that the DNA is loosely packaged. Both the high off-rate of the Abf2p protein and the limited compaction of the complex should aid in allowing enzymes and proteins access to regulatory sites where Diffley and Stillman have showed that "phased" binding of Abf2p occurs (Diffley and Stillman, 1991, 1992). At the same time, this would leave the mtDNA more vulnerable to damage by shear forces, free radicals (Menzies et al., 2002), and nucleases. It is also important to note that the mitochondrial genome in *S. cerevisiae* is circular, rather than linear, and the binding of Abf2p to circular DNA has been shown to form negative supercoils (Diffley and Stillman, 1992) which may impact the compaction of mtDNA through the formation of plectonemes (Strick et al., 2000). Further studies comparing the compaction of DNA by Abf2p and its homolog, h-mtTFA, using both linear and circular DNA, should provide insight into how mtDNA packaging impacts human mitochondrial genome-related diseases.

We would like to thank Dr. Stigter for his calculation of DNA contour lengths, Professor Jodi Nunnari for her comments on the manuscript, and Dr. Michael Colvin for helpful discussions.

Work was performed at Lawrence Livermore National Laboratory (LLNL) under the auspices of the U.S. Department of Energy under contract W-7405-ENG-48 and partially supported by the National Science Foundation Biophotonics Center at University of California at Davis under Agreement No. PHY 0120999. (R.J.B.).

REFERENCES

Alam, T. I., T. Kanki, T. Muta, K. Ukaji, Y. Abe, H. Nakayama, K. Takio, N. Hamasaki, and D. Kang. 2003. Human mitochondrial DNA is packaged with TFAM. *Nucleic Acids Res.* 31:1640–1645.

Baumann, C. G., V. A. Bloomfield, S. B. Smith, C. Bustamante, M. D. Wang, and S. M. Block. 2000. Stretching of single collapsed DNA molecules. *Biophys. J.* 78:1965–1978.

Brewer, L. R., M. Corzett, and R. Balhorn. 1999. Protamine-induced condensation and decondensation of the same DNA molecule. *Science.* 286:120–123.

Brower-Toland, B. D., C. L. Smith, R. C. Yeh, J. T. Lis, C. L. Peterson, and M. D. Wang. 2002. Mechanical disruption of individual nucleosomes reveals a reversible multistage release of DNA. *Proc. Natl. Acad. Sci. USA.* 99:1960–1965.

Caron, F., C. Jacq, and J. Rouviere-Yaniv. 1979. Characterization of a histone-like protein extracted from yeast mitochondria. *Proc. Natl. Acad. Sci. USA.* 76:4265–4269.

Cho, J. H., Y. K. Lee, and C. B. Chae. 2001. The modulation of the biological activities of mitochondrial histone Abf2p by yeast PKA and its possible role in the regulation of mitochondrial DNA content during glucose repression. *Biochim. Biophys. Acta.* 1522:175–186.

Contamine, V., and M. Picard. 2000. Maintenance and integrity of the mitochondrial genome: a plethora of nuclear genes in the budding yeast. *Microbiol. Mol. Biol. Rev.* 64:281–315.

Diffley, J. F., and B. Stillman. 1991. A close relative of the nuclear, chromosomal high-mobility group protein HMG1 in yeast mitochondria. *Proc. Natl. Acad. Sci. USA.* 88:7864–7868.

Diffley, J. F., and B. Stillman. 1992. DNA binding properties of an HMG1-related protein from yeast mitochondria. *J. Biol. Chem.* 267:3368–3374.

Fisher, R. P., T. Lisowsky, M. A. Parisi, and D. A. Clayton. 1992. DNA wrapping and bending by a mitochondrial high mobility group-like transcriptional activator protein. *J. Biol. Chem.* 267:3358–3367.

Garrido, N., L. Griparic, E. Jokitalo, J. Wartiovaara, A. M. Van Der Bliek, and J. N. Spelbrink. 2003. Composition and dynamics of human mitochondrial nucleoids. *Mol. Biol. Cell.* 14:1583–1596.

Jacobs, H. T., S. K. Lehtinen, and J. N. Spelbrink. 2000. No sex please, we're mitochondria: a hypothesis on the somatic unit of inheritance of mammalian mtDNA. *Bioessays.* 22:564–572.

Kao, L. R., T. L. Megraw, and C. B. Chae. 1993. Essential role of the HMG domain in the function of yeast mitochondrial histone HM: functional complementation of HM by the nuclear nonhistone protein NHP6A. *Proc. Natl. Acad. Sci. USA.* 90:5598–5602.

MacAlpine, D. M., P. S. Perlman, and R. A. Butow. 1998. The high mobility group protein Abf2p influences the level of yeast mitochondrial DNA recombination intermediates in vivo. *Proc. Natl. Acad. Sci. USA.* 95:6739–6743.

MacAlpine, D. M., P. S. Perlman, and R. A. Butow. 2000. The numbers of individual mitochondrial DNA molecules and mitochondrial DNA nucleoids in yeast are coregulated by the general amino acid control pathway. *EMBO J.* 19:767–775.

Martin, S. S., E. Pulido, V. C. Chu, T. S. Lechner, and E. P. Baldwin. 2002. The order of strand exchanges in Cre-LoxP recombination and its basis suggested by the crystal structure of a Cre-LoxP Holliday junction complex. *J. Mol. Biol.* 319:107–127.

McGhee, J. D., and P. H. von Hippel. 1974. Theoretical aspects of DNA-protein interactions: cooperative and noncooperative binding of large ligands to a one-dimensional homogeneous lattice. *J. Mol. Biol.* 86:469–489.

Megraw, T. L., and C. B. Chae. 1993. Functional complementarity between the HMG1-like yeast mitochondrial histone HM and the bacterial histone-like protein HU. *J. Biol. Chem.* 268:12758–12763.

Menzies, F. M., P. G. Ince, and P. J. Shaw. 2002. Mitochondrial involvement in amyotrophic lateral sclerosis. *Neurochem. Int.* 40:543–551.

Newman, S. M., O. Zelenaya-Troitskaya, P. S. Perlman, and R. A. Butow. 1996. Analysis of mitochondrial DNA nucleoids in wild-type and a mutant strain of Saccharomyces cerevisiae that lacks the mitochondrial HMG box protein Abf2p. *Nucleic Acids Res.* 24:386–393.

O'Rourke, T. W., N. A. Doudican, M. D. Mackereth, P. W. Doetsch, and G. S. Shadel. 2002. Mitochondrial dysfunction due to oxidative mitochondrial DNA damage is reduced through cooperative actions of diverse proteins. *Mol. Cell. Biol.* 22:4086–4093.

Parisi, M. A., B. Xu, and D. A. Clayton. 1993. A human mitochondrial transcriptional activator can functionally replace a yeast mitochondrial HMG-box protein both in vivo and in vitro. *Mol. Cell. Biol.* 13:1951–1961.

Perkins, T. T., D. E. Smith, R. G. Larson, and S. Chu. 1995. Stretching of a single tethered polymer in a uniform flow. *Science.* 268:83–87.

Richter, C., J. W. Park, and B. N. Ames. 1988. Normal oxidative damage to mitochondrial and nuclear DNA is extensive. *Proc. Natl. Acad. Sci. USA.* 85:6465–6467.

Stigter, D., and C. Bustamante. 1998. Theory for the hydrodynamic and electrophoretic stretch of tethered B-DNA. *Biophys. J.* 75:1197–1210.

Strick, T. R., V. Croquette, and D. Bensimon. 2000. Single-molecule analysis of DNA uncoiling by a type II topoisomerase. *Nature.* 404:901–904.

Wallace, D. C. 2002. Animal models for mitochondrial disease. *Methods Mol. Biol.* 197:3–54.

Wang, M. D., H. Yin, R. Landick, J. Gelles, and S. M. Block. 1997. Stretching DNA with optical tweezers. *Biophys. J.* 72:1335–1346.

Wredenberg, A., R. Wibom, H. Wilhelmsson, C. Graff, H. H. Wiener, S. J. Burden, A. Oldfors, H. Westerblad, and N. G. Larsson. 2002. Increased mitochondrial mass in mitochondrial myopathy mice. *Proc. Natl. Acad. Sci. USA.* 99:15066–15071.

Zelenaya-Troitskaya, O., S. M. Newman, K. Okamoto, P. S. Perlman, and R. A. Butow. 1998. Functions of the high mobility group protein, Abf2p, in mitochondrial DNA segregation, recombination and copy number in Saccharomyces cerevisiae. *Genetics.* 148:1763–1776.

Zimm, B. H. 1998. Extension in flow of a DNA molecule tethered at one end. *Macromolecules.* 31:6089–6098.